

# A global view of the extratropical tropopause transition layer from Atmospheric Chemistry Experiment Fourier Transform Spectrometer O<sub>3</sub>, H<sub>2</sub>O, and CO

M. I. Hegglin,<sup>1</sup> C. D. Boone,<sup>2</sup> G. L. Manney,<sup>3,4</sup> and K. A. Walker<sup>1,2</sup>

Received 19 February 2008; revised 3 November 2008; accepted 26 November 2008; published 4 February 2009.

[1] The global behavior of the extratropical tropopause transition layer (ExTL) is investigated using O<sub>3</sub>, H<sub>2</sub>O, and CO measurements from the Atmospheric Chemistry Experiment Fourier Transform Spectrometer (ACE-FTS) on Canada's SCISAT-1 satellite obtained between February 2004 and May 2007. The ExTL depth is derived using H<sub>2</sub>O-O<sub>3</sub> and CO-O<sub>3</sub> correlations. The ExTL top derived from H<sub>2</sub>O-O<sub>3</sub> shows an increase from roughly 1–1.5 km above the thermal tropopause in the subtropics to 3–4 km (2.5–3.5 km) in the north (south) polar region, implying somewhat weaker troposphere-stratosphere-transport in the Southern Hemisphere. The ExTL bottom extends ~1 km below the thermal tropopause, indicating a persistent stratospheric influence on the troposphere at all latitudes. The ExTL top derived from the CO-O<sub>3</sub> correlation is lower, at 2 km or ~345 K (1.5 km or ~335 K) in the Northern (Southern) Hemisphere. Its annual mean coincides with the relative temperature maximum just above the thermal tropopause. The vertical CO gradient maximizes at the thermal tropopause, indicating a local minimum in mixing within the tropopause region. The seasonal changes in and the scales of the vertical H<sub>2</sub>O gradients show a similar pattern as the static stability structure of the tropopause inversion layer (TIL), which provides observational support for the hypothesis that H<sub>2</sub>O plays a radiative role in forcing and maintaining the structure of the TIL.

**Citation:** Hegglin, M. I., C. D. Boone, G. L. Manney, and K. A. Walker (2009), A global view of the extratropical tropopause transition layer from Atmospheric Chemistry Experiment Fourier Transform Spectrometer O<sub>3</sub>, H<sub>2</sub>O, and CO, *J. Geophys. Res.*, 114, D00B11, doi:10.1029/2008JD009984.

## 1. Introduction

[2] For more than a decade the upper troposphere/lower stratosphere (UTLS) has attracted major research interest owing to its particular role in radiative forcing and chemistry-climate coupling. This is mainly due to strong contrasts between the chemical, dynamical, and radiative properties of the troposphere and the stratosphere [e.g., Shepherd, 2007]. The UTLS encompasses the tropopause, which from a dynamical point of view can be defined by an increase in static stability in the vertical (the thermal tropopause), or by the occurrence of a strong gradient in potential vorticity (PV) in the horizontal (the PV tropopause) [Danielsen, 1959]. The dynamical tropopause represents a

partial barrier to (isentropic) mixing [e.g., Haynes and Shuckburgh, 2000], and hence influences the distribution of chemical tracers in this region, for example as seen in strong gradients in aircraft measurements of H<sub>2</sub>O and O<sub>3</sub> at the tropopause [Browell *et al.*, 1987].

[3] The ozone tropopause defined in terms of either O<sub>3</sub> mixing ratio or vertical gradient of mixing ratio is, however, not coincident with the thermal tropopause, but rather located roughly 800 m below, pointing toward a more complex structure of the tropopause [Bethan *et al.*, 1996]. More recently, in situ aircraft measurements of tropospheric tracers such as CO, excess NO<sub>y</sub>, and H<sub>2</sub>O have revealed that the tropospheric influence extends into the lowermost stratosphere (LMS) [Fischer *et al.*, 2000; Zahn *et al.*, 2000; Hoor *et al.*, 2002, 2004; Pan *et al.*, 2004]. The upper boundary of this tropospheric influence has been found to be limited to around 2–3 km or 20–30 K potential temperature above the local tropopause, and is dependent on the tropopause definition chosen and the chemical tracer used to track the tropospheric influence. These observations helped evolve our understanding of a finite chemical transition layer across the tropopause, with partly tropospheric, partly stratospheric character [Shepherd, 1997; Haynes and Shepherd, 2001]. This region is sometimes referred to as the

<sup>1</sup>Department of Physics, University of Toronto, Toronto, Ontario, Canada.

<sup>2</sup>Department of Chemistry, University of Waterloo, Waterloo, Ontario, Canada.

<sup>3</sup>Jet Propulsion Laboratory, California Institute of Technology, Pasadena, California, USA.

<sup>4</sup>New Mexico Institute of Mining and Technology, Socorro, New Mexico, USA.

extratropical tropopause transition layer (ExTL). The basic existence of the ExTL is qualitatively understood: the large-scale diabatic circulation transports aged stratospheric air downward, and limits the influence of troposphere-to-stratosphere transport events across the extratropical tropopause [Hegglin et al., 2005; Shepherd, 2007]. However, questions still remain about how best to characterize the ExTL, how its depth is controlled by transport processes, how to quantify the relative contributions of quasi-horizontal (isentropic) versus vertical (cross-isentropic) transport in establishing the ExTL, and how these factors might change under climate change. Moreover, our present knowledge comes mainly from aircraft measurements with limited geographical and seasonal coverage.

[4] Recent work by Birner et al. [2002] and Birner [2006], using high-resolution radiosonde data, has shown that the dynamical tropopause also shows a transition layer exhibiting strongly enhanced static stability ( $N^2$ ) values and lying just above the extratropical thermal tropopause. This layer is called the tropopause inversion layer (TIL). Seasonal and latitudinal variations of the TIL have been investigated by Randel et al. [2007] using GPS occultation data, and its depth in the Northern Hemisphere (NH) was quantified by Bell and Geller [2008]. The depths of the TIL and the chemically defined ExTL seem to be similar. Since it has been suggested that the ExTL is statistically centered at the thermal tropopause [Pan et al., 2004], a question that arises is whether there is any special dynamical structure within the tropospheric side of the ExTL.

[5] To address the above topics, it is necessary to compare the ExTL and the TIL over a wider latitude range than hitherto covered by aircraft measurements, to investigate interhemispheric differences, and to study their seasonal behavior. To this end, we use the limb-viewing Atmospheric Chemistry Experiment Fourier Transform Spectrometer (ACE-FTS) on Canada's SCISAT-1 satellite [Bernath et al., 2005], which has provided accurate measurements of numerous chemical species throughout the middle atmosphere with high vertical resolution of  $<1$  km extending into the upper troposphere, and with latitudinal sampling that covers both hemispheres (aircraft campaigns focusing on the ExTL were mainly carried out in the NH). The high quality and capability of the measurements to resolve the small vertical length scales found in the UTLS tracer structure have previously been shown by comparison with aircraft measurements [Hegglin et al., 2008]. Thus, the ACE-FTS measurements provide a valuable data set for investigation of the UTLS.

[6] The paper is structured as follows. Section 2 provides the description of the ACE-FTS data and the derived meteorological products (DMPs) used in this study. In section 3, we describe in detail the methods used, such as tropopause coordinates, tracer-tracer correlations, and relative vertical tracer gradients. We then show results including the climatological seasonal and latitudinal behavior of the tracer distributions in the UTLS (section 4), general features in tracer-tracer correlations (section 5), the latitudinal dependence and seasonal variability of the ExTL, and its relation to characteristic features of the TIL (section 6), and the strong relationship between the static stability structure and the H<sub>2</sub>O distribution as seen using relative vertical H<sub>2</sub>O

gradients (section 7). A summary and discussion are given in section 8.

## 2. Data Description

### 2.1. ACE-FTS Satellite Data

[7] The Atmospheric Chemistry Experiment Fourier Transform Spectrometer (ACE-FTS) on Canada's SCISAT-1 satellite features high resolution ( $0.02\text{ cm}^{-1}$ ) and broad spectral coverage in the infrared (750 to  $4400\text{ cm}^{-1}$ ). The instrument operates in solar occultation mode [Bernath et al., 2005]. The SCISAT-1 satellite was launched into low Earth circular orbit (650 km) with high inclination ( $74^\circ$ ) on 12 August 2003. In solar occultation mode, this orbit provides seasonally varying coverage of the globe, with an emphasis on midlatitudes and the polar regions. Up to 30 occultation events (sunrises or sunsets viewed by the orbiting satellite) occur per calendar day. Science operations for the ACE-FTS began in February 2004.

[8] In this study, we use ACE-FTS version 2.2 CO and H<sub>2</sub>O and “version 2.2 O<sub>3</sub> update” results in the UTLS between February 2004 and May 2007. A total of around 10,000 profiles were obtained during this observation period, with numbers varying between 10 and 100 occultations for each  $5^\circ$  latitude bin, depending on season and latitude (see Figure 5 in section 4.2 for the distributions of the profiles in the different seasons). ACE-FTS results are provided on two altitude grids, a 1-km grid common to all occultations and a “retrieval grid” that varies from occultation to occultation. For this study, we use the measurements on the retrieval grid in the altitude range between 5 and 25 km. The instrument has a 1.25 mrad field-of-view, which subtends an altitude range of 3–4 km at the tangent point (the point of closest approach to the Earth for a solar ray measured by the instrument). However the ACE-FTS instrument collects measurements every 2 s which leads to substantial oversampling in the lower atmosphere. The altitude spacing between measurements varies over the course of the year, governed primarily by the beta angle (the angle between the satellite orbit plane and the Earth-Sun vector) of the occultation. The rate of change of altitude decreases with increasing beta angle, leading to higher vertical sampling for larger beta angles. At low altitudes, refraction effects and clouds also impact the measurement spacing. The altitude spacing in the UTLS varies from about 3 km to less than 1 km [Hegglin et al., 2008]. Validating ACE-FTS against aircraft measurements in the UTLS of the NH midlatitudes has shown the high precision and high vertical resolution of the ACE-FTS retrievals [Hegglin et al., 2008]; the uncertainty introduced by the limited vertical resolution of the ACE-FTS measurements is only around 5–15% in the tropopause region, with higher impact on O<sub>3</sub> than on CO and H<sub>2</sub>O. In order to provide a theoretical explanation for the high vertical resolution of the ACE-FTS, we performed further a quantitative assessment of the effect of vertical smearing. The results are shown in Appendix A. Comparison between ACE-FTS and SPURT aircraft measurements using tropopause based coordinates yielded relative differences of 9% and 12% for CO, 30% and 18% for H<sub>2</sub>O, and 25% and 19% for O<sub>3</sub> in the upper troposphere (UT) and lower stratosphere (LS), respectively, while ACE-FTS O<sub>3</sub> showed smaller differences from ozonesonde mea-

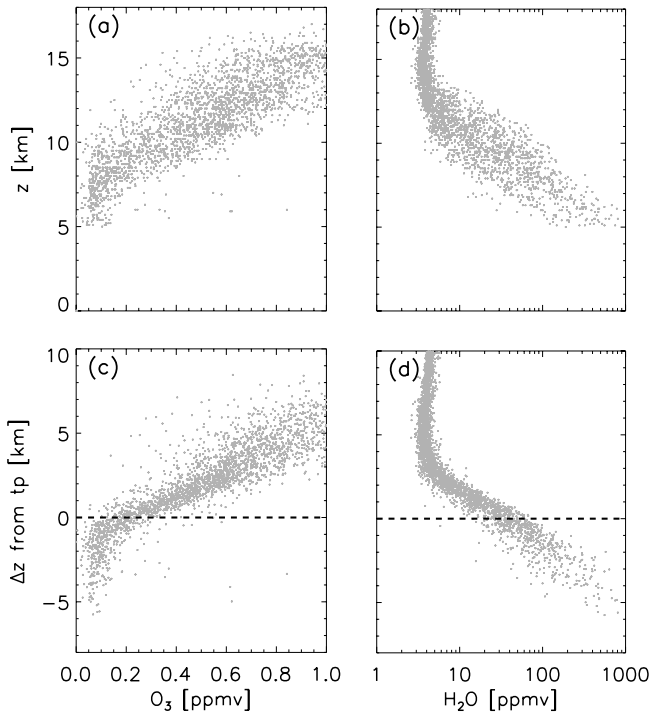


**Figure 1.** Vertical profiles of (a, c)  $O_3$  and (b, d)  $H_2O$  mixing ratios obtained from the ACE-FTS for spring measurements (MAM) during 2005/2006/2007 at latitudes between  $50^\circ\text{N}$  and  $70^\circ\text{N}$ . The profiles are depicted as a function of altitude (Figures 1a and 1b) and of altitude relative to the thermal tropopause (Figures 1c and 1d).

surements of 18% in the UT and 8% in the LS [Hegglin et al., 2008]. Further validation of CO by Clerbaux et al. [2008], of  $O_3$  by Dupuy et al. [2008], and of  $H_2O$  by Carleer et al. [2008] show consistent results. Note that the ACE-FTS  $H_2O$  shows a low bias in the middle to upper troposphere.

## 2.2. Derived Meteorological Products

[9] The thermal tropopause height was derived for each ACE-FTS retrieval using the Reichler et al. [2003] algorithm which is based on the WMO definition, i.e., the lowest level at which the lapse rate drops to  $2 \text{ K km}^{-1}$  or less, and the average lapse rate between this level and all higher levels within 2 km does not exceed  $2 \text{ K km}^{-1}$  [World Meteorological Organization, 1957]. Because ACE-FTS does not retrieve temperature profiles below around 12 km, we use temperature profiles from the Goddard Earth Observing System, Version 5 (GEOS-5) data assimilation system to identify the thermal tropopause. The temperature fields are interpolated onto the ACE measurement locations in time and space. For retrieval locations where the GEOS-5 analyses were not available (before August 2004) we used an older set of derived meteorological products (DMPs) from GEOS Version 4 (GEOS-4). The GEOS-5 analyses are described by Reinecker et al. [2008]. They are provided on 72 model levels from the surface to 0.01 hPa, and a  $0.5^\circ$  latitude by  $2/3^\circ$  longitude grid. The vertical resolution in the tropopause region is about  $1.1\text{--}1.2 \text{ km}$ . The interface between the observations and the Global Circulation Model

(GCM) is performed using the incremental analysis update (IAU) [Bloom et al., 1996], which produces generally smoother analyses. GEOS-5 replaced the GEOS-4 analyses, which are described by Bloom et al. [1996]. The GEOS-4 data used were provided on 55 hybrid ( $\sigma/\text{pressure}$ ) model levels from the surface to 0.01 hPa. The horizontal grid is  $1.0^\circ$  latitude by  $1.25^\circ$  longitude. Both model versions provide 6-hourly average fields centered at 0000, 0600, 1200 and 1800 UT. Besides the standard meteorological variables, GEOS products include an extensive set of fields from the model and assimilation system, including PV calculated internally in the model.

[10] Manney et al. [2008] found little or no relative bias in tropopause locations derived from GEOS-4/5 and European Center for Medium-Range Weather Forecasts (ECMWF) operational analyses in the Arctic region. Those results are supported by an unpublished comparison of tropopause heights along the SPURT aircraft data set between  $30^\circ\text{N}$  and  $70^\circ\text{N}$  derived from the two data sets showing differences in the variability ( $\pm 0.8 \text{ km}$ ), and a small systematic offset of  $-0.2 \text{ km}$  in the GEOS-4/5 values. A comparison between GEOS-4/5 and the tropopause heights determined from the ACE-FTS temperatures (in combination with the Canadian Meteorological Center (CMC) analyses below  $<12 \text{ km}$ ) resulted in a systematic offset of  $-0.06 \pm 0.7 \text{ km}$ . In addition, our comparisons of GEOS-5 with National Centers for Environmental Prediction (NCEP) tropopauses (not shown) for several individual flights of the Stratosphere-Troposphere Analyses of Regional Transport 2008 (START-08) [Pan et al., 2007a] aircraft campaigns show no evidence for a systematic bias.

## 2.3. GPS Radio Occultation Temperature Data

[11] In this study we use the temperature and static stability climatology derived from Global Positioning System (GPS) radio occultation temperatures by Randel et al. [2007]. The GPS temperature data used to establish the climatologies were obtained from the Challenging Minisatellite Payload (CHAMP) in the extratropics between 2001 and 2006. The data were sampled on a 200 m vertical grid. The precision of individual profiles was better than 0.6 K in the altitude region between 5 and 15 km. For a more detailed description and the processing of the data we refer the reader to Randel et al. [2007] and references therein.

## 3. Diagnostic Methods

### 3.1. Tropopause Coordinates

[12] Tropopause coordinates (i.e., using vertical profiles of a variable of interest relative to the tropopause height) are widely used in UTLS studies of both chemical tracer distributions [Logan et al., 1999; Hoor et al., 2004; Pan et al., 2004; Hegglin et al., 2006] and dynamical variables [Birner et al., 2002; Birner, 2006; Randel et al., 2007]. The use of the tropopause coordinate system reduces geophysical variability caused by synoptic-scale and planetary-scale wave activity. These act to smooth the structures found in UTLS data in climatological evaluations using geometric altitude as the vertical coordinate. As seen in Figure 1, by moving from geometric altitude to tropopause coordinates, the vertical profiles of chemical tracers become more compact and reveal a sharp gradient between tropospheric

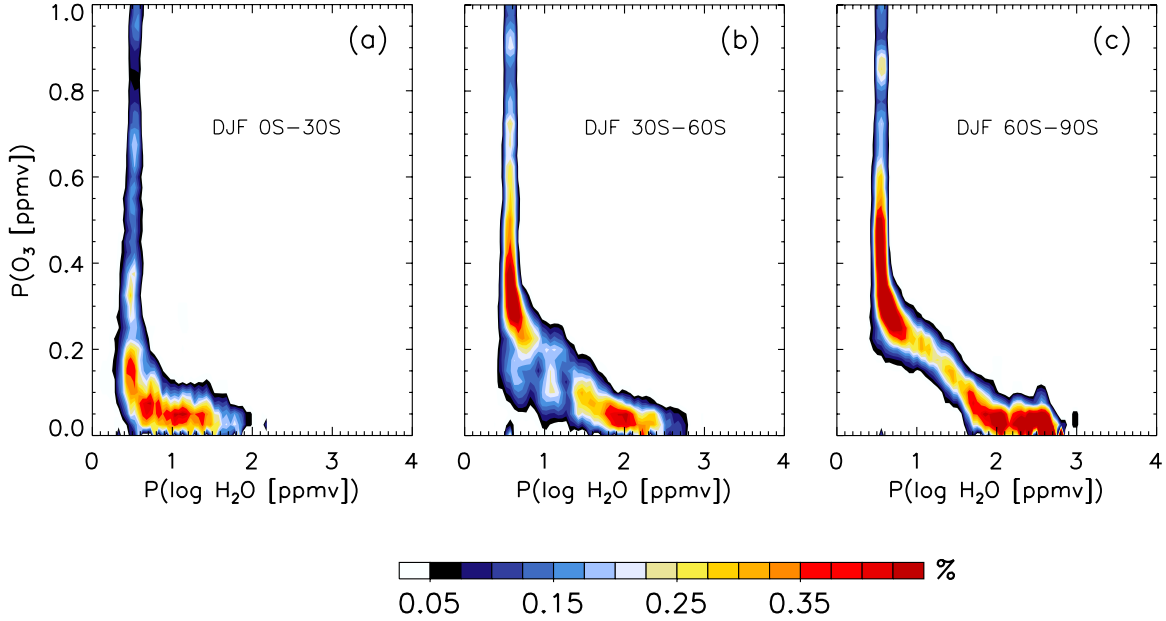


**Figure 2.** Joint probability density function (PDF) of  $\text{H}_2\text{O}$ - $\text{O}_3$  pairs for summer data (all years) between  $-5$  and  $8$  km relative to the tropopause in the SH (a)  $0^\circ\text{S}$ - $30^\circ\text{S}$ , (b)  $30^\circ\text{S}$ - $60^\circ\text{S}$ , and (c)  $60^\circ\text{S}$ - $90^\circ\text{S}$ . The data are weighted with  $1/n(z) \times N$ , where  $n(z)$  is the number of measurements found in the corresponding altitude bin of  $1$  km width in tropopause coordinates, and  $N$  is the total number of measurements used in the evaluation. The data were then binned into  $\text{H}_2\text{O}$  and  $\text{O}_3$  bins with widths of  $0.05$  and  $0.025$  ppmv, respectively.

and stratospheric tracer mixing ratios [see also *Pan et al.*, 2004]. The tropopause coordinate system facilitates the investigation of the specific structure of a given tracer across the tropopause [e.g., *Hoor et al.*, 2004], the validation of the representation of this region in chemistry-climate models [*Pan et al.*, 2007b], and the validation of satellite data with noncoincident aircraft, balloon, or other satellite measurements [*Hegglin et al.*, 2008]. The use of tropopause coordinates is also suggested for trend studies (e.g., of  $\text{O}_3$ ), since trends in the upper troposphere and lower stratosphere are of opposite sign [*Logan et al.*, 1999] and therefore are very likely to be smeared out in a geometrical average.

[13] Observations [*Bethan et al.*, 1996] have shown that when the tropopause is strongly deformed, the ozone tropopause follows the dynamical tropopause more closely than it does the thermal tropopause. This makes sense because while the dynamical tropopause is a Lagrangian coordinate, the thermal tropopause is not [*Wirth*, 2003]. Nevertheless, we use the thermal tropopause as our primary reference in the present study because it allows direct comparison to the ExTL study of *Pan et al.* [2007b], and the TIL studies of *Birner* [2006] and *Randel et al.* [2007]. An additional advantage of the thermal tropopause over the dynamical tropopause is that it can be applied globally, and its calculation requires only the local vertical profile of temperature. A complete understanding of the ExTL would include an understanding of its structure in any coordinate system. In the present (incomplete) state of knowledge, the choice of coordinate is to some extent arbitrary and will be dictated by factors such as the above.

[14] In the tracer-tracer correlation method introduced in the following section, we will compare results for the thermal and the dynamical tropopause (defined by the

$3.5$  PVU surface, with  $1$  PVU =  $10^{-6} \text{ K m}^2 \text{ kg}^{-1} \text{ s}^{-1}$ ). We have chosen the  $3.5$  PVU surface since it is available from the ACE-FTS DMPs and has been found to be close to the thermal tropopause [e.g., *Highwood and Berrisford*, 2000; *Schoeberl*, 2004]. However, the dynamical tropopause has been defined by a range of values between  $1$  and  $4$  PVU [e.g., *Hoerling et al.*, 1991]. Studies by *Hoor et al.* [2004] and *Hegglin et al.* [2006] used the  $2$  PVU surface, which lies closer to the bottom of the ExTL. The results based on the PV definition of the tropopause depend strongly on the choice of PV value.

### 3.2. Tracer-Tracer Correlations

[15] The correlation between a tropospheric and a stratospheric tracer has proven to be an efficient way to identify the chemical transition across the tropopause [*Fischer et al.*, 2000; *Zahn et al.*, 2000; *Hoor et al.*, 2002, 2004; *Pan et al.*, 2004, 2007b]. To determine the depth of the ExTL, we use both the  $\text{H}_2\text{O}$ - $\text{O}_3$  and the  $\text{CO}$ - $\text{O}_3$  correlations. Aircraft measurements have shown the two tracer pairs to yield different results for the ExTL depth (M. Krebsbach et al., Characteristics of the extra-tropical transition layer as derived from  $\text{O}_3$  and  $\text{H}_2\text{O}$  measurements in the UT/LMS during SPURT: II. Extent and seasonal variation, manuscript in preparation, 2009). The reasons for this behavior still need to be investigated, but the shorter lifetime of  $\text{CO}$  than  $\text{H}_2\text{O}$  in the UTLS may be an important factor.

[16] In an ideal atmosphere with no mixing between the troposphere and the stratosphere, the correlation between  $\text{CO}$  (or  $\text{H}_2\text{O}$ ) and  $\text{O}_3$  is expected to show a classical “L shape” [*Fischer et al.*, 2000], with a nearly linear relationship for both tropospheric and stratospheric branches. This feature is indeed observed in the tropics

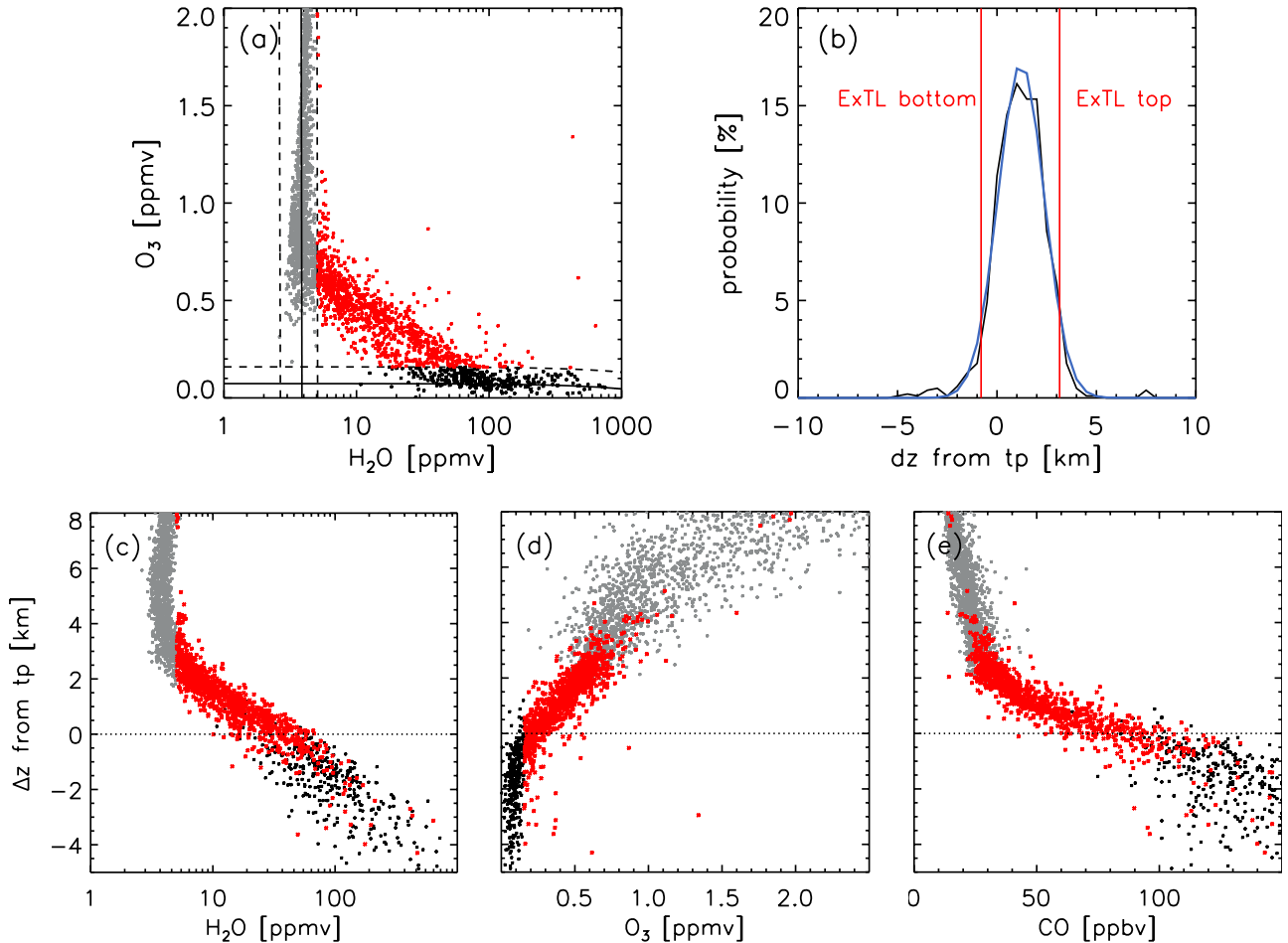


**Figure 3.** (a) H<sub>2</sub>O-O<sub>3</sub> correlation for spring data (all years) between 60°N and 70°N. Black, grey, and red dots depict measurements belonging to the troposphere, stratosphere, and ExTL, respectively. Black lines indicate fits (as explained in text) to tropospheric and stratospheric branches (solid line), and the 4 and 3 standard deviations from those fits, respectively (dashed lines). (b) Probability density function (PDF) of the distance relative to the tropopause of the measurements within the ExTL (black). Blue curve depicts a Gaussian fit to the PDF, and red lines denote top and bottom of the ExTL, which include 95% of all the measurements attributed to the ExTL. (c) Vertical profile of H<sub>2</sub>O in tropopause coordinates and color coded using the above scheme. The horizontal dotted line indicates the thermal tropopause. (d) Same as Figure 3c but for O<sub>3</sub>. (e) Same as Figure 3c but for CO.

for the H<sub>2</sub>O-O<sub>3</sub> correlation (shown as a probability density function (PDF) in Figure 2a), where cross-tropopause mixing is expected to be small and upward motion is associated with dehydration at the tropopause [Brewer, 1949]. At higher latitudes, two-way mixing through synoptic-scale events becomes important [Appenzeller *et al.*, 1996a], and the warmer extratropical tropopause reduces water vapor less efficiently, leading to the erosion of the sharp transition between troposphere and stratosphere as seen in Figures 2b and 2c. As discussed by Hegglin and Shepherd [2007], under such conditions the structure found in tracer-tracer correlations (in the form of scatterplots) mainly reflects sampling, and use of PDFs is preferable. The availability of the ACE-FTS satellite measurements in the UTLS allows the first computation of PDFs in this region. The PDFs in Figures 2b and 2c exhibit minima in the peak within the transition layer, where the maximum in the gradients are found. These minima indicate that the mixing in this region is limited, similar to the minima found in (one-

dimensional or joint) PDFs of stratospheric tracers, which indicate the presence of mixing barriers such as the subtropical edge or the polar vortex [Sparling, 2000; Hegglin and Shepherd, 2007].

[17] Figures 2b and 2c also indicate that the depth of the ExTL increases with latitude, with the top of the transition layer at higher O<sub>3</sub> mixing ratios. As we will see later on, the expected L shape is not achieved in the CO-O<sub>3</sub> correlation because the chemical lifetime of CO is comparable to the transport timescales in the tropical tropopause layer.

[18] To derive the thickness of the ExTL empirically from tracer-tracer correlations, we follow the method suggested by Pan *et al.* [2007b], as illustrated in Figure 3. For a given latitude band and for profiles with tropopause heights <14 km (chosen to exclude air masses with tropical characteristics), the tropospheric branch of the H<sub>2</sub>O-O<sub>3</sub> or CO-O<sub>3</sub> correlation is defined by a linear fit to data with O<sub>3</sub> values ≤100 ppbv. This threshold is chosen at a higher value than the one used by Pan *et al.* [2007b] since the ACE-FTS O<sub>3</sub> measurements

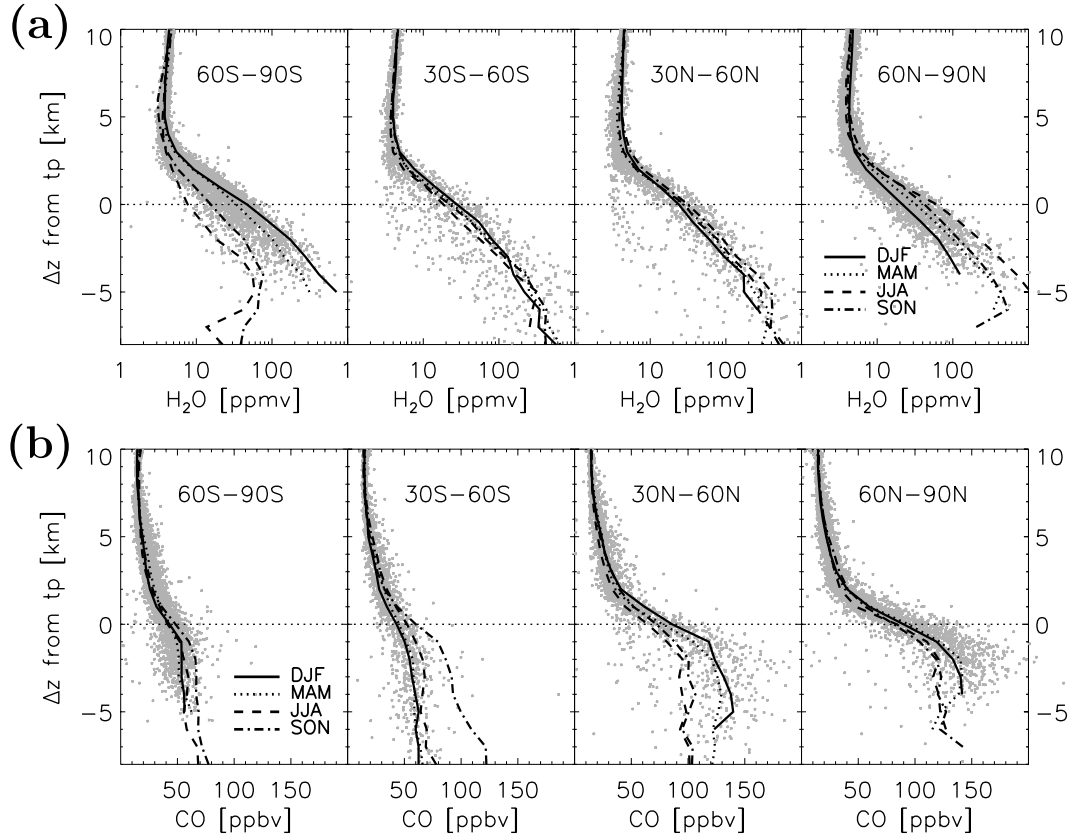


**Figure 4.** Vertical mean profiles of (a)  $H_2O$  and (b) CO in tropopause coordinates (relative to the thermal tropopause) for the latitude bands  $60^{\circ}\text{S}$ – $90^{\circ}\text{S}$ ,  $30^{\circ}\text{S}$ – $60^{\circ}\text{S}$ ,  $30^{\circ}\text{N}$ – $60^{\circ}\text{N}$ , and  $60^{\circ}\text{N}$ – $90^{\circ}\text{N}$  for DJF (solid line), MAM (dotted line), JJA (dashed line), and SON (dash-dotted line). The horizontal dotted line indicates the thermal tropopause. Grey dots show the spring measurements.

exhibit a high bias of  $\sim 18\%$  in the troposphere [Hegglin et al., 2008]. The stratospheric branch, on the other hand, is defined by a second order polynomial fit to data with  $H_2O$  (CO) values  $\leq 5$  (0.03) ppmv and  $O_3$  values  $\leq 3$  ppmv (the latter is to exclude data points above the  $O_3$  maximum). The measurements that lie outside the 4- and 3-sigma ranges of the derived tropospheric and stratospheric fits, respectively, are then deemed to define the ExTL (red points in Figure 3a). We then use a fit to the probability density function of their relative distances from the (thermal or dynamical) tropopause and define the ExTL bottom and top to include 95% of the surface (Figure 3b). Note that, unlike Pan et al. [2007b], we use a logarithmic scale for  $H_2O$ .

[19] To test the robustness of the  $H_2O$ - $O_3$  correlation method for deriving the thickness of the ExTL, we plot  $H_2O$ , CO, and  $O_3$  vertical profiles in tropopause coordinates using the same color code for tropospheric, stratospheric, and ExTL data points as in Figure 3a. The ExTL top is well defined by this method in the tropospheric tracer  $H_2O$ , reaching up to the elbow observed in the  $H_2O$  mixing ratios at around 3 km (Figure 3c). This feature is not as well defined in the stratospheric tracer  $O_3$  (Figure 3d). The ExTL bottom, on the other hand, is well defined in  $O_3$ , but not in  $H_2O$ . This is consistent with the notion of the ExTL exhibiting properties of both the troposphere and the stratosphere. Figure 3e shows that the ExTL defined using the  $H_2O$ - $O_3$  pair does not yield the expected ExTL extent when looking at the CO vertical profile; the strong kink in CO

(which has also been found by Hoor et al. [2004]) is observed at lower altitudes around 2 km rather than at 3 km as the elbow found in  $H_2O$ . However, when the CO- $O_3$  correlation is used to define the ExTL, its extent is well captured in the CO profile.

### 3.3. Relative Vertical Tracer Gradients

[20] We introduce here a new approach for revealing the latitudinal structure of the ExTL based on chemical tracers: the use of relative vertical tracer gradients in tropopause coordinates, which is equivalent to the gradient of the logarithm. The motivation for this approach lies in the strong gradients revealed when plotting  $H_2O$  on a logarithmic scale as seen in Figure 3c, or the strong CO gradient across the tropopause seen in Figure 3e. To this end, the data were binned into 0.25 km height bins relative to the tropopause height and  $5^{\circ}$  latitude bins. The vertical gradient was then calculated and divided by the mean tracer value found in the bin. This procedure resulted in longitudinally averaged cross sections.

### 4. Seasonality and Latitudinal Differences of Vertical Profiles in Tropopause Coordinates

[21] A first impression of the tropospheric influence on the lower stratosphere is obtained by looking at vertical profiles of the tropospheric tracers  $H_2O$  and CO in tropopause coordinates (Figures 4a and 4b). Both tracers show

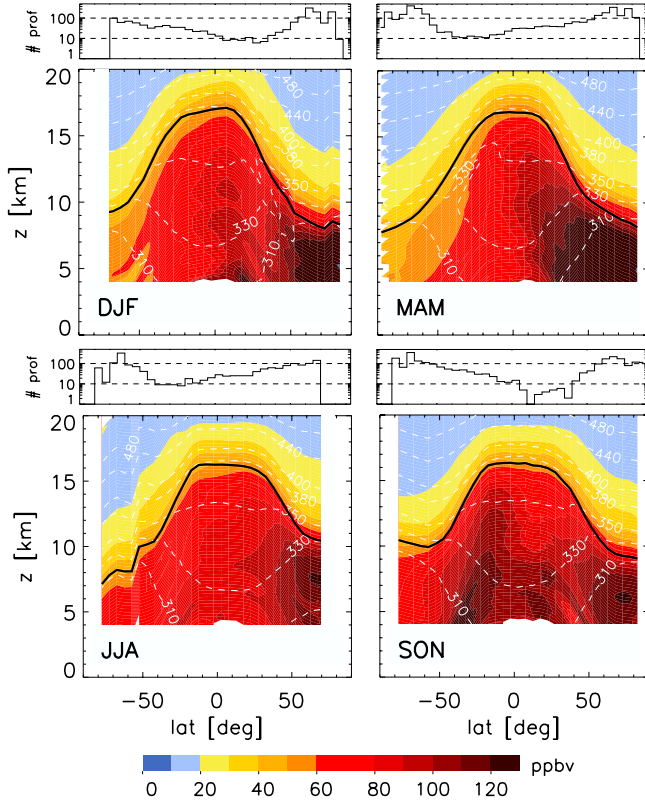


**Figure 5.** Meridional cross sections of seasonally accumulated CO in tropopause-based coordinates and scaled with the seasonal mean tropopause height for DJF, MAM, JJA, and SON. The black solid line denotes the seasonal mean tropopause, and white dashed lines denote the potential temperature levels. Small graphs above main panels indicate the number of vertical profiles in a given 5° latitude band.

large values in the upper troposphere, a region with a pronounced tracer gradient (the ExTL), and smaller values in the lower stratosphere. These profiles are also very useful for model-measurement comparisons to test the capability of (chemistry-climate or chemistry-transport) models to capture the dynamical processes that determine the distinct features observed in tracer distributions in the tropopause region.

#### 4.1. Water Vapor

[22] Figure 4a shows mean  $H_2O$  profiles for different latitude bands and seasons in the extratropics. A clear seasonality is seen only in the high-latitude troposphere, in both hemispheres. The upper troposphere is moister during summer than during winter, a feature that extends into the ExTL. At high latitudes in Southern Hemisphere (SH) winter,  $H_2O$  values are found to be smallest, likely because of the low temperatures in the Antarctic that lead to ice particle formation and subsequent fallout. Tropospheric influence is seen up to 2–3 km above the tropopause, which is approximately the top of the ExTL. It is also up to this height that the variability in the  $H_2O$  profiles is largest (not shown).

#### 4.2. Carbon Monoxide

[23] Figure 4b shows mean CO profiles for different latitude bands and seasons in the extratropics. The profiles reveal the vertical structure of the CO tracer distribution and the large interhemispheric difference in tropospheric CO mixing ratios. Tropospheric CO values are around 55 ppbv in the southern and up to 150 ppbv in the northern high latitudes. The primary reason for the difference is larger emissions from fossil fuel combustion processes in the NH. A distinct seasonality in tropospheric CO with smaller values in summer and autumn, and larger values in winter and spring is observed. This seasonality can be explained by both larger emissions and a longer chemical lifetime of CO (due to less sunlight and limited production of hydroxyl radicals [Taylor *et al.*, 1991]) during winter and spring. There is also a pronounced maximum in tropospheric CO during spring in SH midlatitudes, caused by large CO emissions from biomass burning [Crutzen *et al.*, 1985].

[24] The profiles reveal that the transition between the troposphere and the stratosphere based on CO starts about 1–2 km below the thermal tropopause and occurs over a finite height up to around 2 km above the thermal tropopause. The chemical transition, especially at the bottom of the ExTL seems relatively smooth as opposed to stepwise. A stepwise transition would be expected if isentropic mixing from the subtropical troposphere into the lower stratosphere accounted for the main tropospheric fraction in the ExTL. Such transport would bring (in the NH) air masses with lower CO into the high-latitude ExTL owing to the observed strong pole-equator gradient in tropospheric CO. While this observation does not exclude isentropic mixing it points toward the importance of vertical (i.e., cross-isentropic) mixing through 3D turbulence generated by different dynamical processes as pointed out in a modeling study by Hegglin *et al.* [2005].

[25] The same information as in Figure 4 is provided in a more illustrative way in Figure 5 using zonal mean meridional cross sections of the CO data in tropopause coordinates. Figure 5 reveals a strong latitudinal gradient in the CO in the NH troposphere. Sharp gradients are observed across the tropopause in both the vertical and the horizontal and reveal the ubiquitous existence of the ExTL in the extratropics, extending the findings by Hoor *et al.* [2004] to the SH. The gradients are especially strong at the subtropical jet (typically located near 30° latitude and around 13 km altitude), which has been shown to act as an efficient barrier to mixing [e.g., Haynes and Shuckburgh, 2000; Berthet *et al.*, 2007]. The ExTL lies at higher potential temperatures in summer because of the upward shift of the tropopause due to a weaker Brewer-Dobson circulation.

[26] Figure 5 also shows the effect of “ventilation” [Berthet *et al.*, 2007] or “flushing” [Hegglin and Shepherd, 2007] of the lower stratosphere with tropical tropospheric air. The flushing is reflected in the enhanced transport of younger tropical air masses from just above the subtropical jet to higher latitudes which increases CO mixing ratios between potential temperature levels of 400–440 K by around 10 ppbv. Berthet *et al.* [2007] used trajectory calculations to show that the region between 370 and 410 K experiences a strong tropospheric influence during summer (within 30 days); Hegglin and Shepherd [2007] identified the

same transport process by evaluating the seasonal cycle of the  $O_3-N_2O$  correlation slopes, an indicator of the chemical age of air masses. Hegglin and Shepherd [2007] show that the tropical influence reaches up to  $420 \pm 20$  K and is weaker in the SH, consistent with the CO tracer distribution seen in Figure 5 during DJF.

## 5. General Features in the Tracer-Tracer Correlations

### 5.1. $H_2O-O_3$

[27] Figure 6 shows an overview of the  $H_2O-O_3$  correlations for different seasons and latitude bands, colored according to the measurements' potential temperature calculated from ACE-FTS pressure and GEOS-5 temperature data. The correlations illustrate the seasonal evolution of the ExTL in tracer-tracer space. Equivalent latitude is not used in these figures, since the tracer-tracer correlations are themselves a tool to reveal characteristic tracer features of different air masses caused by specific dynamical and transport processes.

[28] As mentioned in section 3.2, the correlations in the tropics show the theoretical L shape, a result of small cross-tropopause mixing and slow ascent of the air parcels associated with dehydration at the tropopause. The transition between the tropospheric and the stratospheric branches occurs at lower  $H_2O$  mixing ratios during DJF and MAM than during JJA and SON for both hemispheres, reflecting the seasonal cycle in tropical tropopause temperatures with lower temperatures during NH winter. The transition occurs at potential temperature levels between 360 and 380 K. Moving to higher latitudes, mixing between the troposphere and the stratosphere becomes more important, and the warmer extratropical tropopause is less efficient in reducing water vapor. This results in the ExTL showing both tropospheric and stratospheric characteristics. The feature gets broader when moving from middle to high latitudes, except in SH winter where strong  $O_3$  depletion and/or dehydration is shaping the correlations. Comparing the correlations in SH and NH midlatitudes indicates that the transition layer is broader in the NH. The apparent increase in the transition during NH winter and spring with higher  $O_3$  ratios at the top of the transition, however, is mainly due to the seasonal variation of  $O_3$  in the LMS due to the downward flow of stratospheric  $O_3$  which maximizes in late winter and early spring [Logan, 1985; Haynes and Shepherd, 2001; Hegglin et al., 2006].

[29] An interesting feature is seen in the SH polar region (Figure 6, JJA/SON 60°S–90°S) during winter and spring, where the stratospheric branch is split. This is the result of the polar vortex acting as a barrier to mixing between high latitudes and midlatitudes. The branch with lower  $H_2O$  mixing ratios results from dehydration processes within the polar vortex. In the NH midlatitudes during spring (Figure 6, MAM 30°N–60°N), the correlation shows a “high-heel” shape with a dry stratospheric branch reaching down to very low  $O_3$  values. These air masses originate from lower latitudes and show typical tropical characteristics. During summer (Figure 6, JJA 30°N–60°N), more air masses of tropical character can be found at latitudes between 30°N and 60°N because of the poleward shift of the subtropical jet. During summer, the ExTL top experi-

ences a depression to lower  $O_3$  starting at low latitudes and reaching the high latitudes by autumn. This is due to the flushing of the lowermost stratosphere with younger and therefore  $O_3$ -poorer tropical air masses [Hegglin et al., 2006; Hegglin and Shepherd, 2007].

### 5.2. $CO-O_3$

[30] Figure 7 shows the same overview as in Figure 6 but for the  $CO-O_3$  correlation. CO is a “purer” transport tracer than  $H_2O$  since it is not affected by dehydration processes as it crosses the tropopause, and thus yields additional information. The high-heel shape found between 60°S and 90°S during SON implies that, as well as the dehydration described in the previous section,  $O_3$  depletion also contributes to this feature. Only a weak seasonal cycle is observed in the tropics, and rather than an L shape, the correlations form a smooth curve starting at potential temperatures of around 340 K. CO steadily decreases from this point toward its midstratospheric steady state value of around 12–15 ppbv [Flocke et al., 1999]. A similar curvature is observed in the extratropical stratospheric branches, but starting at lower potential temperatures. The relatively short lifetime of CO ( $\sim 3$  months [Hoor et al., 2004]) compared to the timescales of transport processes adds an uncertainty in the interpretation of features in the  $CO-O_3$  correlations.

[31] Figure 7 suggests that the successful use of the  $CO-O_3$  correlation in determining the ExTL depth following the method described in section 3.2 is strongly dependent on a representative sampling of the stratospheric branch which is smoothly curved rather than constant. The fit to the stratospheric branch is therefore likely to be better constrained by the ACE-FTS measurements than by most aircraft measurements, since the latter are limited by the aircraft's ceiling altitude. This discussion emphasizes the need to test the credibility of the fits using vertical tracer profiles as shown in Figures 3d and 3e (recall that Figure 3e was a negative example).

## 6. ExTL Depth

### 6.1. ExTL Depth Derived From the $H_2O-O_3$ and $CO-O_3$ Correlations

[32] To quantify the global ExTL depth we determine the top and bottom of the ExTL following the tracer-tracer correlation method of Pan et al. [2007b], as described in detail in section 3.2. Because the ACE-FTS is an occultation instrument with sampling limited to two latitudes each day, the data are examined over an entire season and over the whole 3-year observation period, to evaluate seasonal rather than monthly means [see also Hegglin and Shepherd, 2007]. This yields a “quasi-climatological” view of the ExTL, which has to be seen as the result of constantly occurring mixing events. Single events may exhibit features in tracer-tracer space which strongly differ from the “quasi-climatological” mean.

[33] Figure 8 shows the top and bottom of the ExTL as distances from the thermal and dynamical tropopauses. These are derived for every 10° latitude band (except the tropics) and each season using both the  $H_2O-O_3$  and the  $CO-O_3$  correlations. Figures 8a and 8b show the annual means of the distances from the thermal tropopause derived

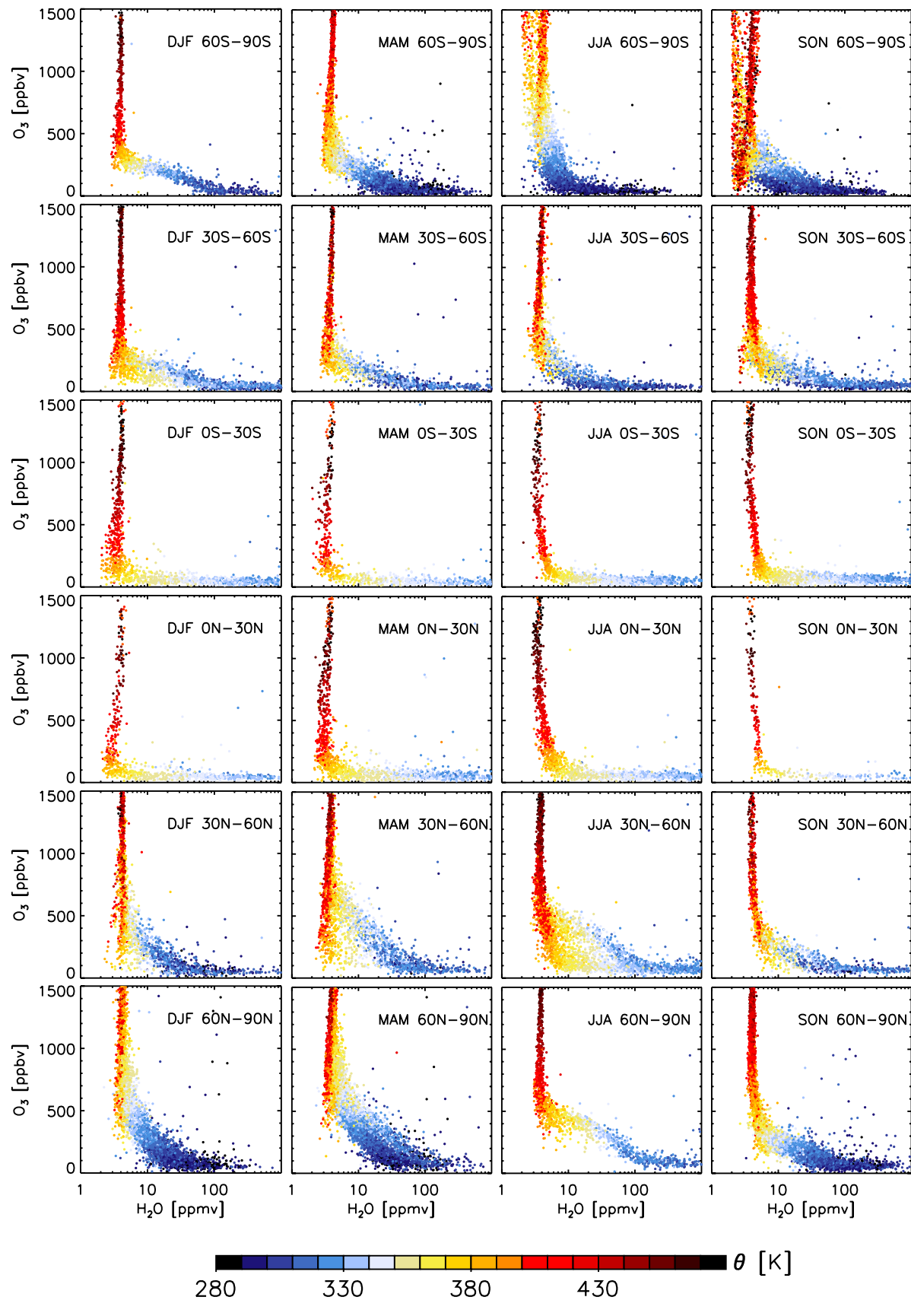


**Figure 6.**  $H_2O-O_3$  correlations for different seasons (left to right) DJF, MAM, JJA, and SON, and for the latitude bands (top to bottom)  $60^{\circ}\text{S}$ - $90^{\circ}\text{S}$ ,  $30^{\circ}\text{S}$ - $60^{\circ}\text{S}$ ,  $0^{\circ}\text{S}$ - $30^{\circ}\text{S}$ ,  $0^{\circ}\text{N}$ - $30^{\circ}\text{N}$ ,  $30^{\circ}\text{N}$ - $60^{\circ}\text{N}$ , and  $60^{\circ}\text{N}$ - $90^{\circ}\text{N}$ . Color code indicates the potential temperature at each data point.

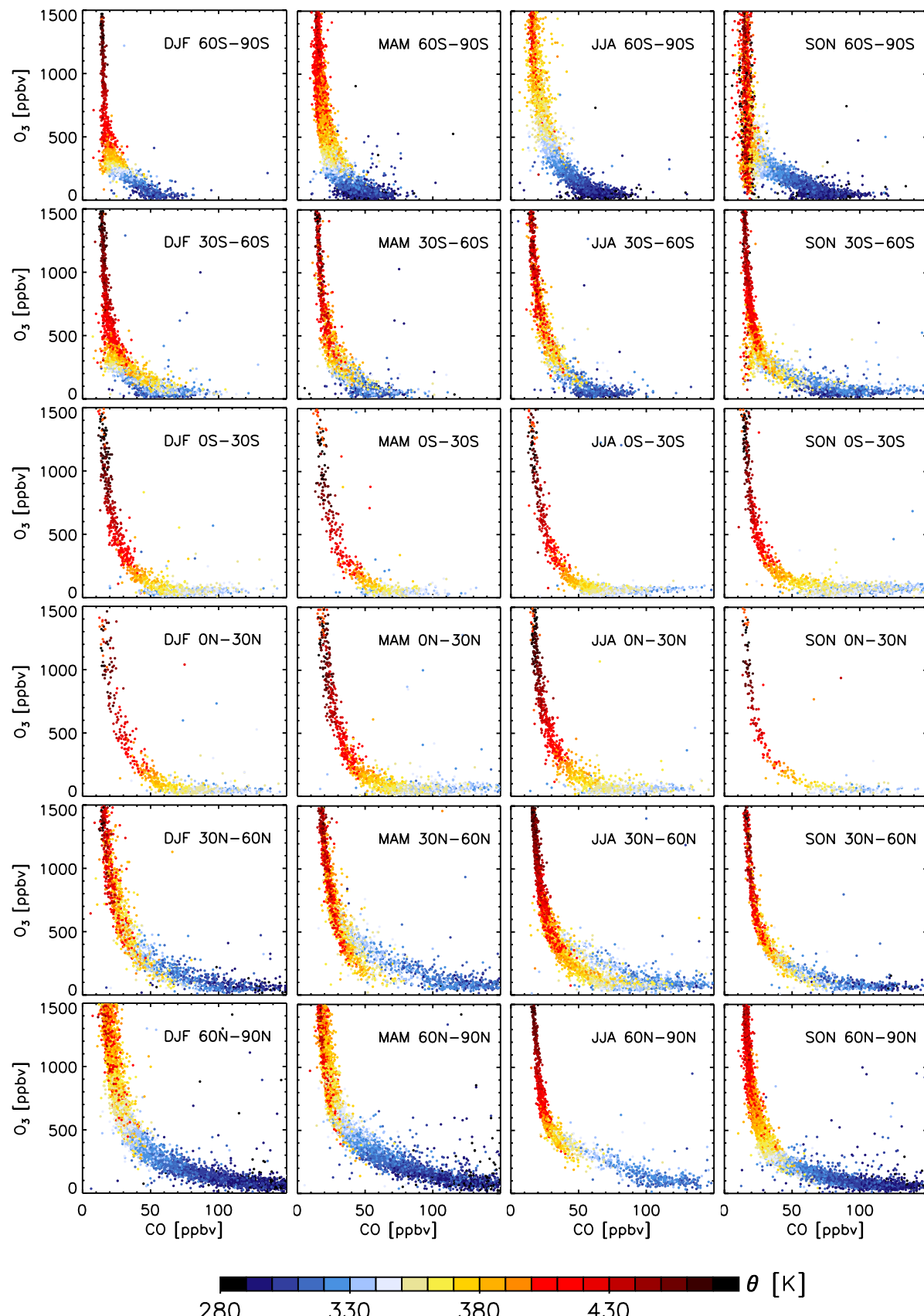


**Figure 7.** Same as Figure 6 but for the CO-O<sub>3</sub> correlation.

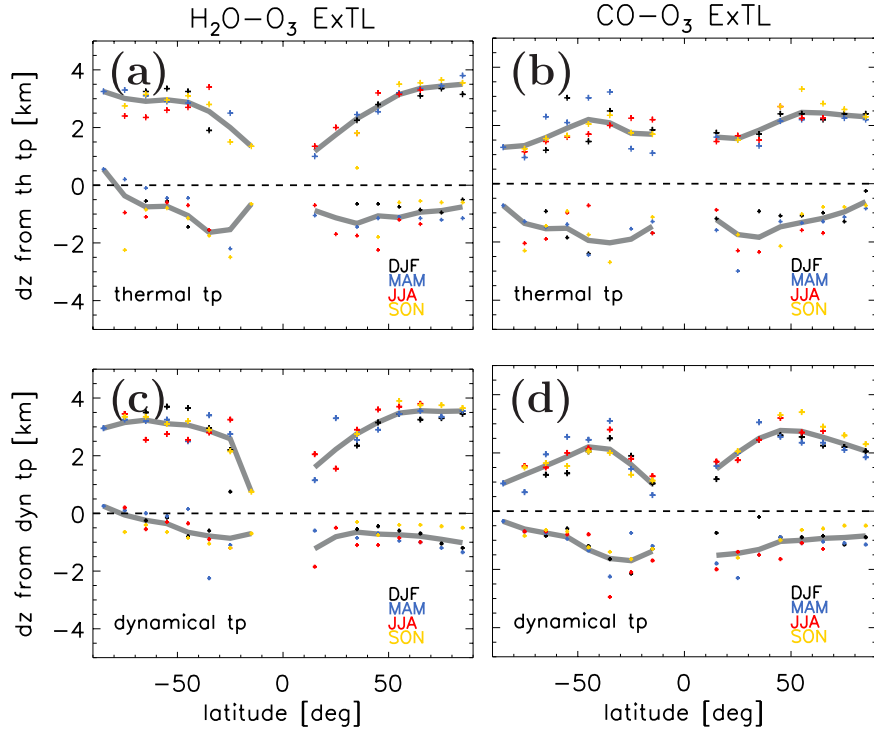


**Figure 8.** Latitudinal dependence of ExTL top and bottom derived from (a, c) the  $\text{H}_2\text{O}-\text{O}_3$ , and (b, d) the  $\text{CO}-\text{O}_3$  correlation method of *Pan et al.* [2007b]; see section 3.2. Figures 8a and 8b show evaluations relative to the thermal tropopause (th tp), and Figures 8c and 8d show evaluations relative to the dynamical tropopause (dyn tp). Top and bottom are calculated for latitude bands of  $10^\circ$  and each season (3-year averages, color coded). Only profiles with tropopause heights  $<14$  km were considered in order to exclude tropical influence. Grey lines denote the annual mean for the whole observation period. Dashed black line indicates the tropopause. The inner tropics  $10^\circ\text{S}$ – $10^\circ\text{N}$  are omitted.

from the two different tracer pairs. The ExTL top derived from  $\text{H}_2\text{O}-\text{O}_3$  is generally higher than that derived from  $\text{CO}-\text{O}_3$  (consistent with Krebsbach et al.’s manuscript in preparation, 2009), and shows a strong increase with latitude with strongest gradients in the subtropics. In the NH, the annual mean ExTL top derived from the  $\text{H}_2\text{O}-\text{O}_3$  increases from about 1–1.5 km in the tropics to 3–4 km in the polar region. In the SH, the annual mean ExTL top increases less, from about 1–1.5 km in the tropics to 2.5–3.5 km in the polar region. The ExTL bottom derived from  $\text{H}_2\text{O}-\text{O}_3$  at NH high latitudes lies around 1 km below the thermal tropopause, and its error bars include the value of 0.8 km derived by *Bethan et al.* [1996]. The ExTL bottom in the SH decreases with increasing latitude. In the SH subtropics the ExTL extends as deep as 1.5 km below the thermal troposphere, and about 0.5 km below at high latitudes.

[34] The ExTL top derived from  $\text{CO}-\text{O}_3$  is roughly constant for both hemispheres with a value of 2 km. The ExTL bottom mostly lies around 0.5 km deeper in the troposphere from that derived from  $\text{H}_2\text{O}-\text{O}_3$ . For both tracer pairs, stratospheric influence on the troposphere appears to maximize in the subtropics with the bottom lying at about –1.5 km. The relatively strong stratospheric influence on the troposphere in the subtropics may be related to a climatological maximum in the distribution of final destinations of deep stratosphere-to-troposphere transport events [*Sprenger and Wernli*, 2003]. *Pan et al.* [2004] concluded

on the basis of evaluations using ER-2 aircraft measurements at  $40^\circ\text{N}$  and  $65^\circ\text{N}$  during the STRAT and POLARIS summer campaigns (1995–1997) that the ExTL is statistically centered around the thermal tropopause. Our findings do not agree with theirs but rather indicate that the thermal tropopause is located somewhat closer to the ExTL bottom, especially at high latitudes. However, note that the location of the ExTL bottom might be biased toward the thermal tropopause by up to 500 m, since we use a higher  $\text{O}_3$  threshold than *Pan et al.* [2007b] to determine the tropospheric branch due to a high bias in the ACE-FTS  $\text{O}_3$  in the troposphere (see section 3.2). The difference in the method applied may therefore partly explain the discrepancy.

[35] Figures 8a and 8b (as well as Figure 4) indicate only a weak seasonality in the ExTL bottom and top locations and hence the depth of the ExTL. At latitudes  $>40^\circ$  in both hemispheres, the ExTL top tends to be lowest in spring and winter, and higher toward autumn. This agrees qualitatively with the finding by *Hoor et al.* [2004] that the ExTL depth is around 20–25 K potential temperature in winter, while it increases to around 30 K in summer. A quantitative comparison of the ExTL depth in these different coordinate systems is more difficult, since the isentropes lie closer together in summer than in winter (this can be seen upon close inspection of Figure 5). Note the very low values for the ExTL top during SH winter; this may arise from both very strong descent and dehydration inside the Antarctic polar vortex. At latitudes  $<40^\circ$ , the interpretation of sea-

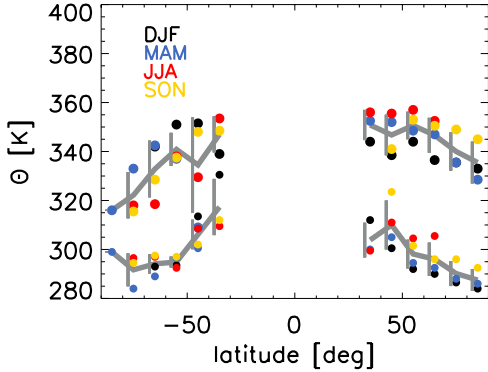


**Figure 9.** ExTL top (large circles) and bottom (small circles) as a function of potential temperature. Colors show different seasons. Grey solid line denotes the annual mean  $\pm 1\sigma$ .

sonality is more complicated owing to the latitudinal shift and seasonal change in strength (and therefore barrier function) of the subtropical jet [Haynes and Shuckburgh, 2000].

[36] Figures 8c and 8d show the same results as Figures 8a and 8b but relative to the dynamical tropopause defined by the 3.5 PVU surface. This PV value has been chosen since it lies closest to the thermal tropopause [e.g., Schoeberl, 2004]. Results obtained using the dynamical tropopause are similar to those using the thermal tropopause. The total ExTL depth is about the same, but the ExTL bottom is somewhat better defined by the dynamical tropopause. Hoor et al. [2004] used the 2 PVU surface as tropopause and found that this value lies closer to the ExTL bottom than does the thermal tropopause.

[37] Figure 9 shows the ExTL top and bottom as a function of potential temperature, to allow comparison with extratropical tropopause studies using that vertical coordinate. For example, Berthet et al. [2007] used Lagrangian trajectory calculations driven by ECMWF winds to investigate tropospheric influence on the UTLS and found that the region below 340 K is strongly influenced by “extratropical” troposphere-to-stratosphere-transport (TST). This agrees well with our findings showing an average of 340–350 K for the ExTL top with a weak seasonal and latitudinal dependence suggesting that the TST processes resolved in the ECMWF analyses are representing the main mechanisms responsible for establishing the ExTL.

[38] The values derived above for the latitudinal dependence of the ExTL top and bottom in the NH compare well with earlier evaluations [Bethan et al., 1996; Hoor et al., 2004; Pan et al., 2004; Berthet et al., 2007; Krebsbach et al., manuscript in preparation, 2009]. However, a study by Pan et al. [2007b] using aircraft  $H_2O$  and  $O_3$  measurements at  $65^\circ$  indicates a sharper transition between the troposphere and the stratosphere, with an ExTL top at only 1.5 km. This apparent inconsistency needs further examination, but may result from the limited sampling of the aircraft during a particular meteorological situation, since tracer behavior across the tropopause has been seen to be different in anticyclonic and cyclonic flows [Bethan et al., 1996], or from longitudinal differences in the ExTL depth that have

yet to be explored. As noted in section 3.2, the method presented here may to some extent be affected by smearing resulting from the use of tropopause heights derived from meteorological analyses with limited vertical resolution or the fact that the fit to the stratospheric data is better constrained in the case of the satellite data (see section 5.2). Finally, as mentioned in section 2, uncertainties and biases in the tropospheric ACE-FTS  $H_2O$  and  $O_3$  retrievals may affect the results presented here, although the ACE-FTS measurements are quite reliable in the lower stratosphere (see Appendix A and Hegglin et al. [2008]).

## 6.2. Comparison Between ExTL and TIL Depth

[39] We now compare the ExTL depth derived from the CO- $O_3$  correlation (Figure 8b) to the maximum in temperature just above the tropopause, which is a main characteristic of the TIL and will be better illustrated in Figure 11 in section 6.3. As can be seen in Figure 10, these heights show a strong correlation in an annual mean. Note that for the temperature maxima only JJA and DJF data were available, while for the ExTL top all seasons were included to get full latitudinal coverage. This inconsistency in the comparison may not influence the results significantly since seasonal variations in the ExTL have been seen to be small (see Figure 8b). However, it could not be shown that such a strong relationship exists between seasonally averaged data. This points toward the importance of different timescales involved in producing the ExTL and the TIL. While the strength of the Brewer-Dobson circulation changes on a seasonal timescale [e.g., Appenzeller et al., 1996b], filamentation processes, which are the prerequisite for mixing in the lowermost stratosphere, occur on timescales of days to weeks [e.g., Haynes and Anglade, 1997], and radiative processes adjust with timescales of weeks to months [e.g., Shine, 1987].

## 6.3. Characteristics of the ExTL and TIL Derived From Vertical Tracer Gradients

[40] We here move on to explore and illustrate characteristic features of the ExTL and TIL using vertical profiles of tracer mixing ratios, their gradients, temperature, and  $N^2$ .

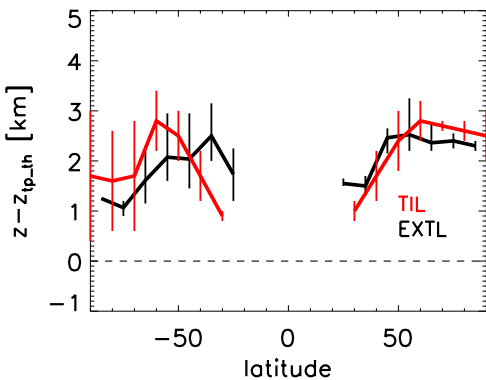


**Figure 10.** Annual mean in the ExTL depth as derived by the CO- $O_3$  correlation (black) and annual mean of the TIL depth defined by the secondary temperature maximum just above the tropopause. Vertical bars indicate maximum and minimum values.

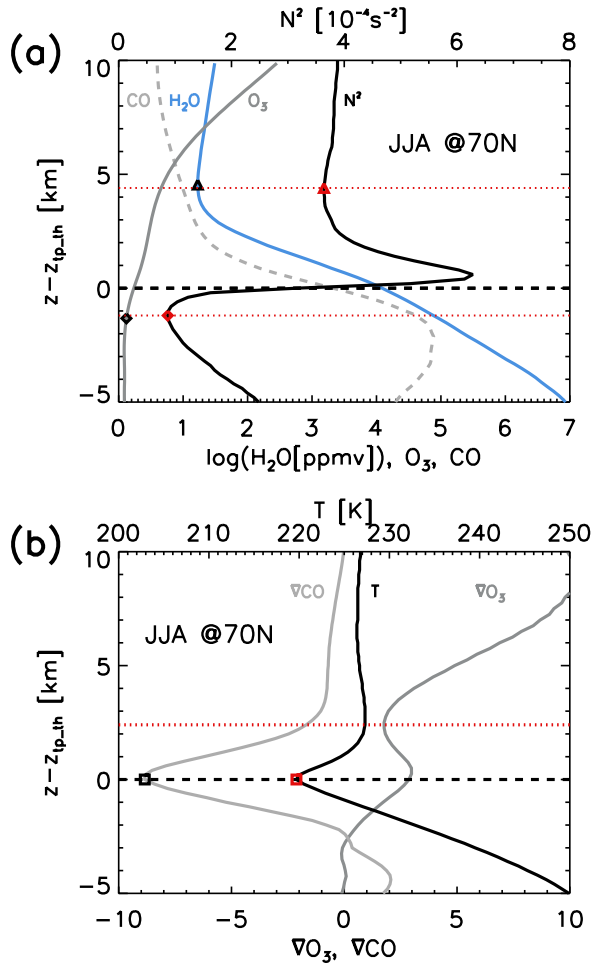


**Figure 11.** Vertical profiles relative to the thermal tropopause: (a)  $N^2$  (black),  $O_3$  (dark grey, ppmv),  $H_2O$  (blue), and  $CO$  (grey dashed line, 20 ppbv) and (b) temperature (black),  $CO$  gradient (light grey, 4 ppbv/km), and  $O_3$  gradient (dark grey, 40 ppbv/km). Dashed black lines denote the tropopause height (0 km). Red dotted lines and symbols indicate height of characteristic features in the TIL and ExTL as discussed in the text. Note the different scaling factors to fit the data on the same scale.

[41] Figure 11 illustrates some chemical and thermal characteristics of the tropopause region using seasonally averaged vertical profiles during summer (JJA) at 70°N. Figure 11a shows zonal mean profiles of  $CO$ ,  $O_3$ ,  $H_2O$ , and  $N^2$ . The TIL top is defined as the minimum in  $N^2$  above the thermal tropopause (red triangle). We here define the TIL bottom to be the local minimum in  $N^2$  found below the tropopause (red diamond). The height of the TIL top seems to correspond to a minimum in the  $H_2O$  vertical profile (black triangle), while the bottom coincides with the height at which  $O_3$  changes significantly from fairly well-mixed tropospheric values to steadily increasing stratospheric values (black diamond). Figure 11b shows the zonal mean profiles of the  $CO$  gradient,  $O_3$  gradient, and temperature. The absolute value of the  $CO$  gradient shows a maximum just at the tropopause (black square), where the temperature has a minimum (red square). The  $O_3$  gradient shows a local maximum at the tropopause, and a minimum about 2.5 km

above the tropopause, coincident with a local maximum in temperature (red square). While these features seem interesting, it remains to be shown whether these relationships depend on latitude and season.

[42] As a first step, we plot the vertical profiles of temperature, and the  $CO$  and  $O_3$  gradients during summer for all latitudes between 30°N and 70°N in 10° latitude bins. The results are shown in Figure 12. Figure 12a shows that the height of the relative maximum in the temperature above the tropopause is increasing with increasing latitude. Figure 12b shows that the absolute maximum in the  $CO$  gradient is a climatological feature over a broad range of latitudes. Figure 12c shows that the relative maxima and minima in the  $O_3$  gradient at and above the tropopause, respectively, are only apparent for latitude bands  $>40^\circ\text{N}$ . The heights of the minima in the  $O_3$  gradient above the tropopause are found to increase with increasing latitude, similarly to the relative maxima in the temperature profiles.

[43] For now, we only focus on the maximum in the absolute  $CO$  gradient and investigate if it is also found in the SH and for both JJA and DJF. Figure 13 shows that absolute maxima in the  $CO$  gradients occur at the thermal tropopause throughout both NH and SH midlatitudes. The relation breaks down in the polar regions during winter, and in the SH subtropical jet region during summer. The maximum in the absolute value of the  $CO$  gradient indicates that the thermal tropopause represents a localized minimum in vertical mixing within the tropopause region. This finding is also supported by Figures 2 and 12c, the latter indicating a localized maximum in the  $O_3$  gradient at least at latitudes  $>40^\circ\text{N}$ .

## 7. Vertical Structure and Seasonal Behavior of the ExTL

[44] Radiative transfer calculations presented by Randel et al. [2007] indicate that the strong gradients in  $H_2O$  and

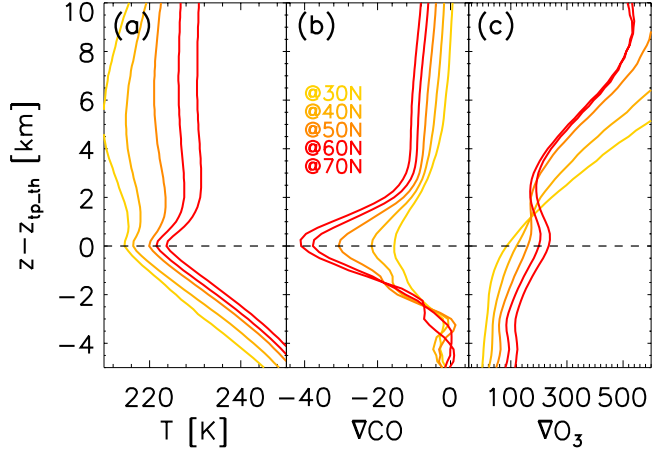


**Figure 12.** Vertical profiles relative to the thermal tropopause for 10° latitude bins between 30°N and 70°N and JJA: (a) temperature, (b)  $CO$  gradient (ppbv/km), and (c)  $O_3$  gradient (ppbv/km). The profiles reveal that the height of the characteristic features in the ExTL and TIL illustrated in Figure 11 change consistently with latitude. For illustrative purposes, the profiles are offset by 1 K, -2 ppbv, and 30 ppbv in Figures 12a, 12b, and 12c, respectively.

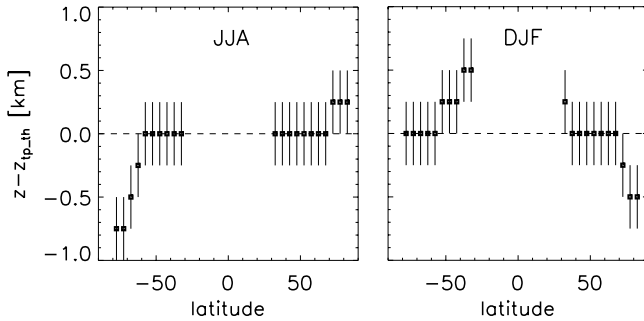


**Figure 13.** Latitudinal dependence of the height of the maximum in the absolute CO gradient for (left) JJA and (right) DJF. All heights are plotted relative to the thermal tropopause height ( $z - z_{tp,th}$ ).

$O_3$  observed across the tropopause may contribute to the temperature inversion just above the tropopause that defines the TIL. The findings by *Randel et al.* [2007] show that  $H_2O$  exerts a cooling effect just above the tropopause, effectively enhancing the inversion and acting in concert with a warming effect by  $O_3$  above.

[45] Figure 14a shows zonally averaged, vertical and latitudinal cross sections of the relative vertical  $H_2O$  gradient in DJF and JJA. For comparison, Figure 14b shows vertical and latitudinal cross sections of  $N^2$  derived from GPS occultation data, taken from *Randel et al.* [2007]. The two quantities exhibit strikingly similar features, suggesting a strong relationship between them. Both the relative vertical  $H_2O$  gradient and  $N^2$  reveal a clear maximum near 1 km above the tropopause; these maxima are strongest during summer in each hemisphere, with the NH exhibiting larger values than the SH. The winter maxima are less pronounced than the summer maxima, and larger values are seen in the NH than the SH. In the SH winter south of  $60^\circ$ s a local minimum is obvious in both quantities, leading to a dipole character with the local maxima found at midlatitudes. However, the distribution of the relative  $O_3$  gradient (Figure 14c) does not exhibit the same structure, but a maximum just below the tropopause along with a local minimum between 1 and 4 km above the tropopause during summer. During winter, the  $O_3$  gradients decrease steadily with height. The presence of the relative maxima just below the tropopause at all latitudes supports the relation between  $O_3$  and  $N^2$  presented in Figure 11a.

[46] The above comparison shows that the seasonal changes in and scales of the relative vertical  $H_2O$  gradient and the  $N^2$  structure of the TIL are similar. This result provides observational support for the hypothesis of *Randel et al.* [2007] that the vertical structure of  $H_2O$  plays a radiative role in forcing and maintaining the TIL.

## 8. Summary and Discussion

[47] A climatological evaluation of the global characteristics of the ExTL using CO,  $O_3$ , and  $H_2O$  measurements from the limb-viewing Atmospheric Chemistry Experiment Fourier Transform Spectrometer (ACE-FTS) on Canada's SCISAT-1 satellite [*Bernath et al.*, 2005] is presented, along

with analysis of the relationship of the ExTL to the TIL. ACE-FTS has provided accurate measurements of numerous chemical species throughout the middle atmosphere with high vertical resolution (better than 1 km in the UTLS), and with nearly global latitudinal sampling. The results thus extend our knowledge derived from previous aircraft campaigns in terms of latitude, altitude and seasonal coverage.

[48] The study of vertical profiles (and zonal mean cross sections) in tropopause coordinates reveals the existence of an ExTL on the global scale. In the lower stratosphere, only small seasonal variations for both CO and  $H_2O$  are found, with the exception of the NH summer at potential temperature levels between 400 and 440 K, where the CO stratospheric background value of 12–15 ppbv is increased by  $\approx 10$  ppbv. This increase in CO supports the finding of *Hegglin and Shepherd* [2007] based on the  $O_3$ - $N_2O$  correlation, that the lowermost stratosphere is being flushed during summer with younger air from the tropics. In the troposphere seasonal variations are more pronounced, in  $H_2O$  because of its dependence on temperature, and in CO because of its dependence on emissions and available sunlight (which determines its photochemical oxidation rate). The seasonal variability propagates into the ExTL, indicating the connection between the ExTL and the troposphere just below. The propagation of the seasonal cycle into the ExTL is consistent with the study by *Hoor et al.* [2004], who showed that the seasonal cycle in  $CO_2$  within the first 20 K (potential temperature) above the dynamical tropopause is in phase with the tropospheric cycle; however the amplitude is attenuated indicating the influence of older stratospheric air. CO also shows a strong north–south gradient because of much larger emissions by fossil fuel burning in the NH than in the SH.

[49] The nearly global coverage of the ACE-FTS also allowed us to compare  $H_2O$ - $O_3$  and CO- $O_3$  correlations in the tropics and the SH where few previous data are available. A classical L shape [*Fischer et al.*, 2000] is found in the  $H_2O$ - $O_3$  correlation in the tropics, where vertical transport across the tropopause is mainly upward into the stratosphere and the low tropopause temperatures determine the amount of  $H_2O$  entering the stratosphere by dehydration. In the extratropics, however, the transition is rather gradual, reflecting the influence of stratosphere-troposphere exchange processes and higher tropopause temperatures causing weaker dehydration. On the other hand, the CO- $O_3$  correlation does not achieve the typical L shape, mainly owing to the chemical lifetime of CO which is comparable to the transport timescales on which troposphere-to-stratosphere transport is occurring.

[50] The  $H_2O$ - $O_3$  and CO- $O_3$  correlation method of *Pan et al.* [2007b] was refined and used to derive the ExTL depth in terms of the distance of its top and bottom from the thermal and dynamical tropopauses. The ExTL derived from  $H_2O$ - $O_3$  extends roughly from around 1 km below to 3 km above the tropopause with some latitudinal and seasonal differences. Its top shows an increase from roughly 1–1.5 km above the thermal tropopause in the subtropics to 3–4 km (2.5–3.5 km) in the north (south) polar region, implying somewhat weaker troposphere-stratosphere-transport in the SH. The fact that the ExTL bottom extends 1 km below the thermal tropopause, indicates a persistent stratospheric

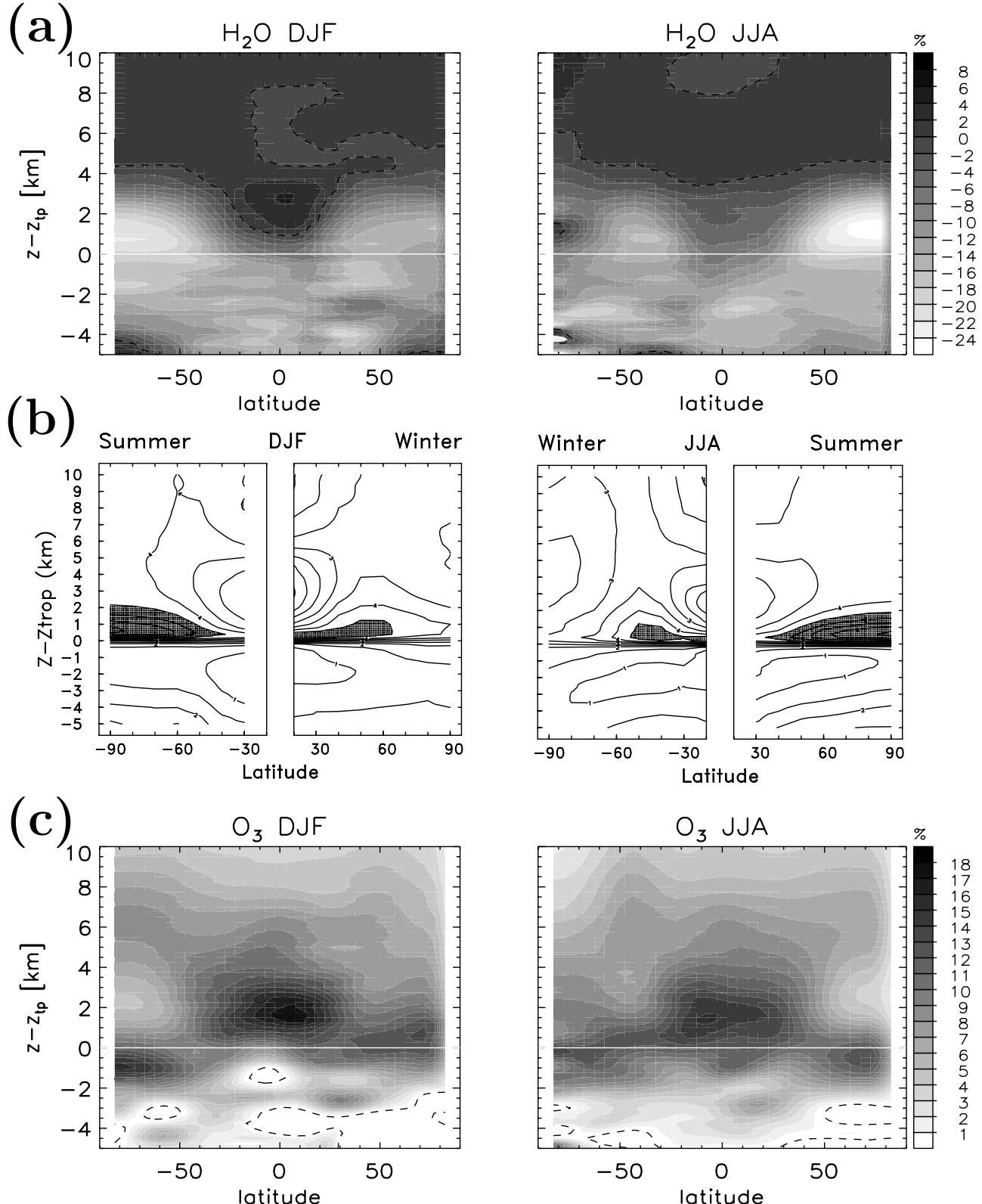


**Figure 14.** Relative vertical gradients (in %/km) of (a)  $H_2O$  and (c)  $O_3$  from the ACE-FTS. White areas indicate maxima in the absolute value of the gradient. (b) Climatological static stability ( $N^2$ ) from GPS radio occultation data taken from *Randel et al.* [2007] (reproduced by permission of the American Meteorological Society). Grey shaded areas indicate maxima in  $N^2$ . All data are shown in tropopause coordinates. (left) Data for DJF. (right) Data for JJA.

influence on the troposphere at all latitudes. This influence is stronger in the subtropics, where the bottom extends 1.5 km below the tropopause. The ExTL top derived from the H<sub>2</sub>O-O<sub>3</sub> pair shows only a weak seasonality, being slightly ( $\sim 0.5$  km) higher during summer and autumn.

[51] The ExTL derived from the CO-O<sub>3</sub> correlation extends roughly from around 1.5 below to 2 km above the thermal tropopause without a strong latitudinal dependence. The ExTL top is found near 2 km or  $\sim 345$  K (1.5 km or  $\sim 335$  K) in the NH (SH). Seasonal variations are small, but show somewhat higher values during summer/autumn than during winter/spring. The ExTL derived by CO-O<sub>3</sub> is thinner than the one derived from the H<sub>2</sub>O-O<sub>3</sub> pair, confirming the results from Krebsbach et al. (manuscript in preparation, 2009). The reason for this behavior remains unclear since the main mechanisms that produce the ExTL are still under investigation. However, CO has a shorter lifetime than H<sub>2</sub>O (thus transport signatures may be obscured by chemical changes), and because of the exponential decrease in H<sub>2</sub>O across the tropopause even very small amounts of troposphere-to-stratosphere transport will produce a signature in H<sub>2</sub>O in the lower stratosphere.

[52] The differences between the ExTL depth relative to the thermal and dynamical tropopauses are found to be small in this climatological view using the 3.5 PVU value as dynamical tropopause. However, the results depend on the PV value chosen: 2 PVU has been previously found to mark the bottom of the ExTL [Hoor et al., 2004; Hegglin et al., 2006; Krebsbach et al., 2006].

[53] Our results also show that the annual average height of the ExTL top derived from the CO-O<sub>3</sub> correlation is strongly related to the height of the maximum in temperature above the tropopause and not as might have been expected by the minimum in N<sup>2</sup> which has been used to define the TIL depth [Bell and Geller, 2008]. The relationship between the temperature maximum and the ExTL top in single seasons is less obvious, which points to differences in the relative importance of dynamical, chemical, and radiative processes, which act on different timescales, in establishing the TIL and ExTL.

[54] The ExTL has been interpreted as the result of diabatic mixing driven by recurrent wave-breaking events in the tropopause region that result from baroclinic instability and produce filaments of tropospheric air advected into the stratosphere and vice versa. These filaments, which exhibit different chemical and radiative characteristics, are then mixed by three-dimensional turbulence generated by dynamical processes such as gravity-wave breaking and clear-air turbulence [e.g., Hegglin et al., 2005]. Comparison of our results with a Rossby wave breaking (RWB) climatology [Hitchman and Huesmann, 2007] reveals that the seasonality and location of strong and frequent RWB events correspond qualitatively well to latitudinal and interhemispheric variations in the ExTL. In particular, there is a maximum in frequency and strength of RWB events at high latitudes between 320 and 350 K (i.e., the tropopause region and 2–3 km above), and RWB events become less frequent and less intense toward the subtropics. RWB events are, furthermore, more frequent and more intense in the NH than in the SH, consistent with our finding that the ExTL is thinner in the SH than in the NH. The link between the

RWB events and the ExTL depth is provided by Berthet et al. [2007]. They show using Lagrangian trajectory calculations that extratropical troposphere-to-stratosphere exchange, which is caused primarily by RWB, extends up to 340–350 K in the extratropical lower stratosphere consistent with our results derived from the CO-O<sub>3</sub> correlation of the ExTL depth in theta coordinates.

[55] We further explored the chemical and thermal characteristics of the tropopause region using vertical profiles in tropopause coordinates of tracer mixing ratios, their gradients, temperature, and N<sup>2</sup>. Our evaluations reveal a pronounced maximum in the absolute value of the vertical CO gradient directly at the thermal tropopause, which indicates that the thermal tropopause represents a localized minimum in vertical mixing within the tropopause region. Haynes and Shuckburgh [2000] showed that the tropopause acts as a barrier to horizontal (quasi-isentropic) mixing; our results complete this view by showing that it also acts as a barrier to vertical mixing.

[56] Finally, the comparison between zonally and seasonally averaged relative vertical gradients of H<sub>2</sub>O and N<sup>2</sup> reveals that the two variables show very similar patterns and vertical scales. This result provides observational support for the hypothesis of Randel et al. [2007] that the vertical structure of H<sub>2</sub>O plays a radiative role in forcing and maintaining the TIL.

[57] The analyses presented in this paper provide a suite of validation diagnostics for testing the ability of Chemistry-Climate Models (CCMs) to simulate the ExTL with its latitudinal and seasonal behavior. The ACE-FTS measurements can be used as a valuable data set for the same purpose and also allow us to test the representativeness of diagnostics derived from geographically limited aircraft measurements.

## Appendix A

[58] Because of the strong decrease with altitude of H<sub>2</sub>O in the tropopause region, there is a possibility that the depth of the ExTL derived from the H<sub>2</sub>O measurements may be contaminated by the troposphere. In particular, the concern is that if, along the line of sight (LOS), the tropopause rises above the altitude in question then even a small amount of tropospheric H<sub>2</sub>O would strongly influence the retrieved value. In other words, horizontal integration would introduce a vertical smearing which would be dominated by the influence of the troposphere, which (if true) would mean that the stratospheric part of the transition layer would be an artifact of the retrieval.

[59] To quantify the importance of this effect, we use horizontal profiles of tropopause height from flights of the SPURT aircraft campaign (which are available at high horizontal resolution [Engel et al., 2006]) to compute the likelihood of a given tropopause displacement as a function of the horizontal displacement, as a probability density function (PDF). As expected, these PDFs broaden as the horizontal displacement increases. Integrating these PDFs along the line of sight (out to 100 km horizontal displacement) produces the combined PDF shown by the grey dashed curve (labeled unshifted) in Figure A1. The value of 100 km is chosen because the contributions to the LOS

value beyond that distance are assigned to a higher tangent height in the retrieval process. The tropopause displacements are mainly limited to a few hundred meters. However, one should also adjust for the fact that the altitude of the LOS increases quadratically away from the tangent point. This is accounted for in the black solid curve. Now it can be seen that it is extremely unlikely that along the LOS one is seeing air that is at a lower altitude (relative to the tropopause) than the tangent height.

[60] The question is whether the negative tail of the distribution in Figure A1 might nevertheless introduce a high bias in the retrieved H<sub>2</sub>O because of the high values in the troposphere. We study the impact of this vertical smearing on the retrieval of a hypothetical water vapor profile that is decreasing exponentially with a scale height of 1 km (see ACE-FTS profiles just above the tropopause in Figure 5). This is the fastest rate of decrease found anywhere in the profiles, so is a “worst case” result in terms of tropospheric influence. The result is shown in Figure A2, and is to be interpreted as the likelihood of sampling air with a water vapor value as indicated. The observed value would be the average over the entire PDF. Influence from lower altitudes shows up as values larger than unity, while influence from higher altitudes shows up as values smaller than unity. We see basically no influence from lower altitudes, but a quite significant influence from higher altitudes. (The latter is accounted for in the retrievals assuming a linear altitude dependence of the retrieved variable.) In any case, however, this certainly excludes the possibility of the ExTL in H<sub>2</sub>O being an artifact of contamination by the troposphere.

[61] **Acknowledgments.** ACE is funded primarily by the Canadian Space Agency (CSA). We thank the CSA for access to the data. This research has been supported by the Canadian Foundation for Climate and Atmospheric Sciences and the CSA through the C-SPARC network. Many thanks go to Bill Randel and Fei Wu for providing the GPS data, and to William Daffer for his work in providing the derived meteorological

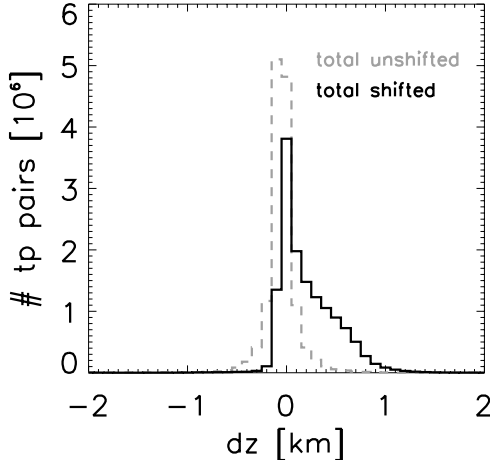


**Figure A1.** Probability density function of tropopause displacements along 36 SPURT flights obtained during four different seasons between 2001 and 2003 over Europe (grey dashed line, total unshifted), integrating over all horizontal distances up to 100 km. Black curve shows the same, but taking into account that the altitude of the ACE-FTS LOS increases quadratically away from the tangent point.

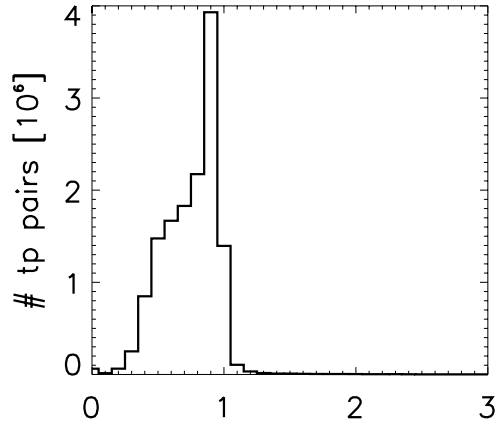


**Figure A2.** Same as in Figure A1 but weighted using an exponential function. Values smaller than unity indicate stratospheric influence, while values larger than unity indicate tropospheric influence.

products. Work at the Jet Propulsion Laboratory, California Institute of Technology, was done under contract with the National Aeronautics and Space Administration. Thanks go to Ted Shepherd for assistance with Appendix A, and to Matt Hitchman and Peter Hoor for helpful comments on an earlier version of the manuscript.

## References

- Appenzeller, C., H. C. Davies, and W. A. Norton (1996a), Fragmentation of stratospheric intrusions, *J. Geophys. Res.*, 101(D1), 1435–1456.
- Appenzeller, C., J. R. Holton, and K. H. Rosenlof (1996b), Seasonal variation of mass transport across the tropopause, *J. Geophys. Res.*, 101(D10).
- Bell, S. W., and M. A. Geller (2008), Tropopause inversion layer: Seasonal and latitudinal variations and representation in standard radiosonde data and global models, *J. Geophys. Res.*, 113, D05109, doi:10.1029/2007JD009022.
- Bernath, P. F., et al. (2005), Atmospheric Chemistry Experiment (ACE): Mission overview, *Geophys. Res. Lett.*, 32, L15S01, doi:10.1029/2005GL022386.
- Berhet, G., J. G. Esler, and P. H. Haynes (2007), A Lagrangian perspective of the tropopause and the ventilation of the lowermost stratosphere, *J. Geophys. Res.*, 112, D18102, doi:10.1029/2006JD008295.
- Bethan, S., G. Vaughan, and S. J. Reid (1996), A comparison of ozone and thermal tropopause heights and the impact of tropopause definition on quantifying the ozone content of the troposphere, *Q. J. R. Meteorol. Soc.*, 122, 929–944.
- Birner, T. (2006), Fine-scale structure of the extratropical tropopause region, *J. Geophys. Res.*, 111, D04104, doi:10.1029/2005JD006301.
- Birner, T., A. Dörnbrack, and U. Schumann (2002), How sharp is the tropopause at midlatitudes?, *Geophys. Res. Lett.*, 29(14), 1700, doi:10.1029/2002GL015142.
- Bloom, S., L. Takacs, A. da Silva, and D. Ledvina (1996), Data assimilation using incremental analysis updates, *Mon. Weather Rev.*, 124, 1256–1271.
- Boone, C. D., et al. (2005), Retrievals for the Atmospheric Chemistry Experiment Fourier Transform Spectrometer, *Appl. Opt.*, 44, 7218–7231.
- Brewer, A. W. (1949), Evidence for a world circulation provided by the measurements of helium and water vapour distribution in the stratosphere, *Q. J. R. Meteorol. Soc.*, 75, 351–363.
- Browell, E., E. Danielsen, S. Ismail, G. Gregory, and S. Beck (1987), Tropopause fold structure determined from airborne lidar and in situ measurements, *J. Geophys. Res.*, 92(D2), 2112–2120.
- Carleer, M., et al. (2008), Validation of water vapour profiles from the Atmospheric Chemistry Experiment (ACE), *Atmos. Chem. Phys. Discuss.*, 8, 4499–4559.
- Clerbaux, C., et al. (2008), CO measurements from the ACE-FTS satellite instrument: Data analysis and validation using ground-based, airborne and spaceborne observations, *Atmos. Chem. Phys.*, 8, 2569–2594.
- Crutzen, P. J., A. C. Delany, J. Greenberg, P. Haagenson, L. Heidt, R. Lueb, W. Pollock, W. Seiler, A. Wartburg, and P. Zimmerman (1985), Tropospheric chemical composition measurements in Brazil during the dry season, *J. Atmos. Chem.*, 2, 233–256.
- Danielsen, E. F. (1959), The laminar structure of the atmosphere and its relation to the concept of a tropopause, *Arch. Meteorol. Geophys. Bioklimatol. Ser. B*, 11, 3H.

- Dupuy, E., et al. (2008), Validation of ozone measurements from the Atmospheric Chemistry Experiment (ACE), *Atmos. Chem. Phys. Discuss.*, 8, 2513–2656.
- Engel, A., et al. (2006), Highly resolved observations of trace gases in the lowermost stratosphere and upper troposphere from the SPURT project: An overview, *Atmos. Chem. Phys.*, 6, 283–301.
- Fischer, H., F. G. Wienhold, P. Hoor, O. Buijok, C. Schiller, P. Siegmund, M. Ambaum, H. A. Scheeren, and J. Lelieveld (2000), Tracer correlations in the northern high latitude lowermost stratosphere: Influence of cross-tropopause mass exchange, *Geophys. Res. Lett.*, 27(1), 97–100, doi:10.1029/1999GL010879.
- Flocke, F., et al. (1999), An examination of chemistry and transport processes in the tropical lower stratosphere using observations of long-lived and short-lived compounds obtained during STRAT and POLARIS, *J. Geophys. Res.*, 104(D21), 26,625–26,642.
- Haynes, P., and J. Anglade (1997), The vertical-scale cascade in atmospheric tracers due to large-scale differential advection, *J. Atmos. Sci.*, 54, 1121–1136.
- Haynes, P., and T. G. Shepherd (2001), Report on the SPARC tropopause workshop, *SPARC News.*, 17, 3–10.
- Haynes, P., and E. Shuckburgh (2000), Effective diffusivity as a diagnostic of atmospheric transport: 2. Troposphere and lower stratosphere, *J. Geophys. Res.*, 105(D18), 22,795–22,810.
- Hegglin, M. I., and T. G. Shepherd (2007), O<sub>3</sub>-N<sub>2</sub>O correlations from the Atmospheric Chemistry Experiment: Revisiting a diagnostic of transport and chemistry in the stratosphere, *J. Geophys. Res.*, 112, D19301, doi:10.1029/2006JD008281.
- Hegglin, M. I., D. Brunner, T. Peter, J. Staehelin, V. Wirth, P. Hoor, and H. Fischer (2005), Determination of eddy diffusivity in the lowermost stratosphere, *Geophys. Res. Lett.*, 32, L13812, doi:10.1029/2005GL022495.
- Hegglin, M. I., et al. (2006), Measurements of NO, NO<sub>y</sub>, N<sub>2</sub>O, and O<sub>3</sub> during SPURT: Implications for transport and chemistry in the lowermost stratosphere, *Atmos. Chem. Phys.*, 6, 1331–1350.
- Hegglin, M. I., C. D. Boone, G. L. Manney, T. G. Shepherd, K. A. Walker, P. F. Bernath, W. H. Daffer, P. Hoor, and C. Schiller (2008), Validation of ACE-FTS satellite data in the upper troposphere/lower stratosphere (UTLS) using non-coincident measurements, *Atmos. Chem. Phys.*, 8, 1483–1499.
- Highwood, E. J., and P. Berrisford (2000), Properties of the Arctic tropopause, *Q. J. R. Meteorol. Soc.*, 126, 1515–1532.
- Hitchman, M. H., and A. S. Huesmann (2007), A seasonal climatology of Rossby wave breaking in the layer 330–2000 K, *J. Atmos. Sci.*, 64, 1922–1940.
- Hoerling, M. P., T. K. Schaak, and A. J. Lenzen (1991), Global objective tropopause analyses, *Mon. Weather Rev.*, 119, 1816–1831.
- Hoor, P., H. Fischer, L. Lange, J. Lelieveld, and D. Brunner (2002), Seasonal variations of a mixing layer in the lowermost stratosphere as identified by the CO-O<sub>3</sub> correlation from in situ measurements, *J. Geophys. Res.*, 107(D5), 4044, doi:10.1029/2000JD000289.
- Hoor, P., C. Gurk, D. Brunner, M. I. Hegglin, H. Wernli, and H. Fischer (2004), Seasonality and extent of extratropical TST derived from in-situ CO measurements during SPURT, *Atmos. Chem. Phys.*, 4, 1427–1442.
- Krebsbach, M., C. Schiller, D. Brunner, G. Günther, M. I. Hegglin, D. Mottaghy, M. Riese, N. Spelten, and H. Wernli (2006), Seasonal cycles and variability of O<sub>3</sub> and H<sub>2</sub>O in the UT/LMS during SPURT, *Atmos. Chem. Phys.*, 6, 109–125.
- Logan, J. (1985), Tropospheric ozone: Seasonal behavior, trends, and anthropogenic influence, *J. Geophys. Res.*, 90(D6), 10,463–10,482.
- Logan, J. A., et al. (1999), Trends in the vertical distribution of ozone: A comparison of two analyses of ozonesonde data, *J. Geophys. Res.*, 104(D21), 26,373–26,399.
- Manney, G. L., et al. (2008), The high Arctic in extreme winters: Vortex, temperature, and MLS Trace gas evolution, *Atmos. Chem. Phys.*, 8, 505–522.
- Pan, L. L., W. J. Randel, B. L. Gary, M. J. Mahoney, and E. J. Hintsa (2004), Definitions and sharpness of the extratropical tropopause: A trace gas perspective, *J. Geophys. Res.*, 109, D23103, doi:10.1029/2004JD004982.
- Pan, L. L., et al. (2007a), Chemical behavior of the tropopause observed during the Stratosphere-Troposphere Analyses of Regional Transport experiment, *J. Geophys. Res.*, 112, D18110, doi:10.1029/2007JD008645.
- Pan, L. L., J. C. Wei, D. E. Kinnison, R. R. Garcia, D. J. Wuebbles, and G. P. Brasseur (2007b), A set of diagnostics for evaluating chemistry-climate models in the extratropical tropopause region, *J. Geophys. Res.*, 112, D09316, doi:10.1029/2006JD007792.
- Randel, W. J., F. Wu, and P. Forster (2007), The extratropical tropopause inversion layer: Global observations with GPS data, and a radiative forcing mechanism, *J. Atmos. Sci.*, 64, 4489–4496.
- Reichler, T., M. Dammer, and R. Sausen (2003), Determining the tropopause height from gridded data, *Geophys. Res. Lett.*, 30(20), 2042, doi:10.1029/2003GL018240.
- Reinecker, M. M., et al. (2008), The GEOS-5 data assimilation system: A documentation of GEOS-5.0, *Tech. Rep. 104606 V27*, NASA Goddard Space Flight Cent., Greenbelt, Md.
- Schoeberl, M. R. (2004), Extratropical stratosphere-troposphere mass exchange, *J. Geophys. Res.*, 109, D13303, doi:10.1029/2004JD004525.
- Shepherd, T. G. (1997), Transport and mixing in the lower stratosphere: A review of recent developments, *SPARC News.*, 9, 5–19.
- Shepherd, T. G. (2007), Transport in the middle atmosphere, *J. Meteorol. Soc. Jpn.*, 85B, 165–191.
- Shine, K. P. (1987), The middle atmosphere in the absence of dynamical heat fluxes, *Q. J. R. Meteorol. Soc.*, 113, 603–633.
- Sparling, L. C. (2000), Statistical perspectives on stratospheric transport, *Rev. Geophys.*, 38, 417–436.
- Sprenger, M., and H. Wernli (2003), A northern hemispheric climatology of crosstropopause exchange for the ERA15 time period (1979–1993), *J. Geophys. Res.*, 108(D12), 8521, doi:10.1029/2002JD002636.
- Taylor, J. A., G. P. Brasseur, R. Zimmerman, and R. J. Cicerone (1991), A study of the sources and sinks of methane and methyl chloroform using a global three-dimensional Lagrangian tropospheric tracer transport model, *J. Geophys. Res.*, 96(D2), 3013–3044.
- Wirth, V. (2003), Static stability in the extratropical tropopause region, *J. Atmos. Sci.*, 60, 1395–1409.
- World Meteorological Organization (1957), Meteorology—A three-dimensional science, *WMO Bull.*, 6, 134–138.
- Zahn, A., et al. (2000), Identification of extratropical two-way troposphere-stratosphere mixing based on CARIBIC measurements of O<sub>3</sub>, CO, and ultrafine particles, *J. Geophys. Res.*, 105(D1), 1527–1535.

C. D. Boone, Department of Chemistry, University of Waterloo, 200 University Avenue West, Waterloo, ON N2L 3G1, Canada. (cboone@acebox.uwaterloo.ca)

M. I. Hegglin and K. A. Walker, Department of Physics, University of Toronto, 60 St. George Street, Toronto, ON M5S 1A7, Canada. (michaela@atmosphysics.utoronto.ca; kwalker@atmosphysics.utoronto.ca)

G. L. Manney, Jet Propulsion Laboratory, MS 183-701, 4800 Oak Grove Drive, Pasadena, CA 91109, USA. (Gloria.L.Manney@jpl.nasa.gov)